DOE/ID/13331-2

Dilute Oxygen Combustion

Phase 2 Final Report

Yong Wang

Hisashi Kobayashi

September 2005

Work Performed Under Contract No. DE-FC36-95ID13331

For
U.S. Department of Energy
Assistant Secretary for
Energy Efficiency and Renewable Energy
Washington, DC

By
Praxair, Inc.
Tonawanda, NY

DOE/ID/13331-2

Dilute Oxygen Combustion

Phase 2 Report

Yong Wang

Hisashi Kobayashi

September 2005

Work Performed Under Contract No. DE-FC36-95ID13331

For
U.S. Department of Energy
Assistant Secretary for
Energy Efficiency and Renewable Energy
Washington, DC

By
Praxair, Inc.
Tonawanda, NY

DILUTE OXYGEN COMBUSTION

Phase 2 Report

September 2005

Work Performed Under Contract No. DE-FC36-95ID13331

For
U.S. Department of Energy
Assistant Secretary for
Energy Efficiency and Renewable Energy
Washington, DC

By
Praxair, Inc.
Industrial Application & Healthcare Research and Development
Tonawanda, NY
Yong Wang, Ph.D.
Hisashi Kobayashi, Ph.D., Principal Investigator

ACKNOWLEDGEMENTS

This work was conducted with the financial support of the U.S. Department of Energy, Office of Industrial Technologies, under Cooperative Agreement DE-FC36-95ID13331. Technical and administrative guidance was provided by Bill Prymak, U.S. Department of Energy, Golden Field Office. Funding was also provided by Praxair, Inc.

The technical inputs and excellent cooperation of Praxair engineer (Juan Li), technologists (Robert Miller and Nicholas Alexander) and manager (Lee Rosen) were instrumental to the successful completion of this project.

TABLE OF CONTENTS

LIST OF FIGURES

LIST OF TABLES

EXECUTIVE SUMMARY

Dilute Oxygen Combustion (DOC) [1-4] is a unique combustion concept to achieve uniform temperature distribution and extremely low emissions of NOx in industrial furnaces. Fuel and air or oxygen streams are injected separately at high velocities into a furnace in order to induce a large amount of in-furnace flue gas recirculation. The high-velocity air/oxygen jets mix rapidly with the surrounding furnace gas and create hot diluted oxidant streams. The high velocity fuel jets entrain and react with this hot diluted oxidant, producing large combustion zones with low peak flame temperatures, resulting in uniform temperature distribution and low NOx emissions. Oxygen is a preferred oxidant as the fuel efficiency of the furnace is substantially improved and the combination of the low flame temperature and the low nitrogen concentration reduces NOx emissions well below those achievable with air-based low NO_x combustion processes.

The basic combustion characteristics of the Dilute Oxygen Combustion (DOC) were studied in detail in laboratory furnaces in Phase I [5]. Commercial scale DOC burners were developed and installed and operated in a steel reheat furnace in Phase III [6]. The design options and efficiencies of new steel reheat furnaces using the DOC technology were studied in Phase IV [7]. In this phase of the project, research was focused on improving thermal efficiency of DOC burners. Oxygen-fired DOC burners generally provide a substantially better thermal efficiency than air-fired burners due to the elimination of nitrogen in combustion air. However, the sensible heat loss of flue gas in high-temperature process furnaces is still a significant fraction even in oxy-fuel combustion. Development of an efficient heat recovery method using rapid cycle regenerators for oxy-fuel fired DOC burners was the main goal of this phase. The maximum amount of heat recovery by oxygen preheating in a regenerator is typically limited to about 50% of the sensible heat of its own flue gas due to the relatively low heat capacity [1]. Natural gas can be both physically heated and chemically reformed in a regenerator to recover a substantially greater amount of heat [4]. A mixture of natural gas and recycled flue gas undergoes endothermic carbon dioxide and steam reforming reactions in the regenerator. This natural gas heat recovery approach, termed "thermochemical regeneration", was considered to provide an elegant solution to the waste

heat recovery problem for oxy-fuel combustion. In order to explore the potential for different regenerative heat recovery approaches, the following tests were carried out:

(1) A bench-top reforming reaction bed was built to simulate the thermochemical regenerator and tested to study the feasibility and the kinetics of natural gas reforming reactions with oxy-fuel flue gas;
(2) Pilot-scale regenerators were built and nitrogen preheating tests were conducted to determine the thermal characteristics of the regenerators and to define the safe operation boundaries for oxygen preheating;
(3) Pilot-scale oxygen preheating tests were carried out to measure the thermal heat recovery capability by oxygen;
(4) Pilot-scale natural gas reforming tests were conducted to measure the heat recovery capability by the thermochemical regenerator concept.

The following results were obtained from the tests.

(1) Bench-Scale Tests

A bench-scale packed bed was set up and the effects on methane conversion of bed temperature, gas residence time, the mixing ratio of flue gas to methane, and the type of bed materials were investigated. Highest methane conversion was 35% and achieved at the conditions of 22 SCFH (standard cubic feet per hour at 60 °F and 1 atm) of reactant flow rate, 2300 ºF peak bed temperature, 60 ms residence time, and 1:1 mixing ratio in a packed bed of alumina beads. The dry product compositions were 47.5% H_2, 16.2% CO, 29.9% CH_4 and 4.1% CO_2. Calculated heat absorbed by the gas mixture from the bed was approximately 2210 Btu/hour, consisting of 1460 Btu/hour of sensible heat and 750 Btu/hour of reaction heat.

(2) Pilot-Scale Nitrogen Preheating Tests

Physical heat transfer characteristics of pilot scale regenerators were investigated using nitrogen. Nitrogen preheat temperature above 2000 ºF was obtained at the furnace temperature of 2400 ºF. The thermal ratio, which is a measure of the ratio of the actual heat recovered to the sensible heat available in exhaust gas, increased as the nitrogen flow rate increased and exceeded 0.9 under some conditions. When the ratio of the exhaust gas flow

rate and the nitrogen flow rate was kept constant, the cycle time did not have a strong impact on the bed temperature profile. The observed bed temperature profiles were in reasonable agreement with those predicted by the Λ-Π heat transfer model.

(3) Pilot-Scale Oxygen Preheating Tests

Oxygen was preheated up to 2000 ºF in the pilot-scale regenerator under various flow rates and cycle times of exhaust gas and oxygen. A heat recovery rate per regenerator bed of about 14,000 Btu/hr was achieved by using an average oxygen flow rate of 300 SCFH and an average flue gas flow rate about 230 SCFH. The results represent about 50% heat recovery from the oxy-fuel continuous firing conditions of 150 SCFH of natural gas per bed with about 60% of the flue gas exhausted through each regenerator bed. Thermal ratio was about 0.95, resulting in the average flue gas temperature after the regenerator of about 180 ºF. The experimental results on the bed temperature profile were in reasonable agreements with predictions by the Λ-Π model.

(4) Pilot Scale Natural Gas Reforming Tests

The same pilot scale regenerators were used for thermochemical heat recovery. As with the oxygen thermal heating tests, various flow rates and cycle times of exhaust gas were investigated at different mixture ratios of natural gas and recycled flue gas. In addition, six different bed materials and configurations were tested.

The relative contributions of the thermal and chemical heat recovery varied widely depending on the operating conditions. When high-average bed temperatures were maintained by increasing the ratio of the exhaust gas flow rate to the flow rate of the mixture of natural gas and recycled flue gas, as much as 50% of the total heat recovered was due to endothermic chemical reactions. The feasibility of the thermochemical heat recovery concept was demonstrated by reforming natural gas and recycled flue gas in the pilot-scale regenerators. Gross heat exchange rates over 20,000 Btu/hr were achieved in some cases, but the net heat exchange rate was below 15,000 Btu/hr for the test conditions. Flue gas temperature after the regenerator was generally higher for these tests and further improvements may be possible for commercial systems. A unique feature of the

thermochemical regenerator is to recover extra waste heat from other burners and the tests demonstrated heat recovery capability over 150% of the waste heat available from its own flue gas. Of the six different bed materials and configurations, the composite bed of cordierite honeycomb and 304 stainless steel beads showed the best results. Some soot was found in the exhaust gas pipe and the problem has to be solved for the design of commercial regenerative systems.

1. INTRODUCTION

Dilute Oxygen Combustion (DOC) is a unique combustion concept to achieve uniform temperature distribution and extremely low emissions of NOx in industrial furnaces. Fuel and air or oxygen streams are injected separately at high velocities into a furnace in order to induce a large amount of in-furnace flue gas recirculation. The high-velocity air/oxygen jets mix rapidly with the surrounding furnace gas and create hot diluted oxidant streams. The high-velocity fuel jets entrain and react with this hot diluted oxidant, producing large combustion zones with low-peak flame temperatures, resulting in uniform temperature distribution and low NOx emissions. Oxygen is a preferred oxidant as the fuel efficiency of the furnace is substantially improved and the combination of the low flame temperature and the low nitrogen concentration reduces NOx emissions well below those achievable with air-based low NO_x combustion processes.

Oxygen-fired DOC burners generally provide a substantially better thermal efficiency than air-fired burners due to elimination of nitrogen in combustion air. The total exhaust gas flow rate is dramatically reduced and, hence, the sensible heat loss through flue gas. However, in high-temperature processes (especially in furnaces with flue gas temperature above 2000 °F), the sensible heat loss through flue gas is still a significant fraction even in oxy-fuel combustion. Improving DOC burner thermal efficiency is the main goal of this phase.

Recuperative and regenerative heat exchangers are the two most commonly used heat recovery devices [8]. In a recuperator, hot and cold fluids flow continuously and exchange heat through a dividing wall or a heat transfer surface. In a regenerator, hot and cold fluids flow alternatively into the same heat exchange chamber and exchange heat with the heat storing media, which is typically a bed of refractory material. Cyclic operation of at least two regenerator beds is required for continuous operation. Due to the high temperature and often corrosive nature of combustion flue gases, the material selection for recuperator heat transfer walls is a challenging issue. The maximum air preheat temperature by a state-of-the-art high temperature metal recuperator is currently limited to about 850 °C. Regenerators generally

have higher heat transfer efficiencies than recuperators and the maximum air preheat temperature can reach as high as 1300 °C with ceramic heat transfer media. For this reason, the regenerative heat recovery approach was selected for this study.

The sensible heat in the flue gas from oxy-fuel combustion can be transferred to either oxygen or fuel for heat recovery. Based on theoretical calculations, however, preheating of oxygen or fuel gas alone is not capable of recovering all the waste heat in flue gas. Fuel gas thermochemical reforming, an innovative idea, was previously proposed and patented to overcome this limitation [9]. Flue gas from oxy-fuel combustion contains mainly steam, carbon dioxide, and a small amount of excess oxygen and nitrogen. If the flue gas is mixed with fuel, such as natural gas, carbon dioxide and steam-reforming reactions can occur under a sufficiently high temperature. Since the reforming reactions are endothermic, the heat recovery capability of natural gas is substantially enhanced as compared with the simple physical heating of natural gas. High-temperature regenerator beds, if heated to a high temperature by oxy-fuel combustion flue gas, would provide the required reforming reaction conditions. In order to explore the potential for different regenerative heat recovery approaches, the following tests have been carried out:

(1) A bench-top thermochemical regenerator was built to study the feasibility and the kinetics of natural gas reforming reactions with oxy-fuel flue gas;

(2) Pilot-scale nitrogen preheating tests were conducted to find the safe operation boundaries for regenerators;

(3) Pilot-scale oxygen preheating experiments were carried out to explore the oxygen heat recovery capability;

(4) Pilot-scale thermochemical regenerators were tested to examine the natural gas heat recovery capability.

In the following sections, the development of regenerative heat recovery devices for oxy-fuel combustion is described, with a main focus on thermochemical regeneration.

2. NATURAL GAS THERMOCHEMICAL REFORMING BENCH TOP TEST

Overview

In the furnace flue gas, the major species of oxy-fuel combustion are CO_2 and H_2O. Both of them can react with natural gas to generate CO and H_2, as illustrated in Equation (1) and (2), which are known as CO_2 reforming and steam reforming [10, 11].

$$CO_2 + CH_4 \rightarrow 2CO + 2H_2 \quad (1)$$

$$H_2O + CH_4 \rightarrow CO + 3H_2 \quad (2)$$

The commercial methane steam and CO_2 reformers use externally heated reformer tubes filled with catalyst so that the reforming reactions can occur at relatively low temperatures (1400 °F to 1600 °F) at an elevated pressure [12, 13]. Most catalysts are expensive and also vulnerable to poisoning by the trace impurities in the feed gases, such as hydrogen sulfide in natural gas [14, 15]. For applications for the thermochemical regenerators, the cost and life-time associated with the catalysts become a major issue as the flue gas from a high-temperature industrial furnace typically contains many particulates and volatiles. Since some of the reforming reactions can take place without catalysts [16, 17] under a sufficiently high temperature and a full conversion of natural gas to H_2 and CO is not required for the regenerator applications [9], it was decided to focus on non-catalytic thermochemical regenerators. The objective of the bench-top test was to prove the feasibility of the natural gas thermochemical reforming concept and to develop the kinetic information to design the pilot-scale regenerators. The reactants were methane and oxy-fuel combustion products (carbon dioxide, steam and etc.) and the reaction products were methane, carbon dioxide, steam, carbon monoxide, hydrogen and other minor species. Different operation conditions were investigated to maximize the natural gas conversion to hydrogen and carbon monoxide.

Experimental Setup

In order to simulate the actual furnace operation of the thermochemical regenerators, the bench-scale test facility was made of two key sub-systems: a flue gas generator and a simulated thermochemical regenerator bed. A schematic drawing of the entire system is

shown in Figure 1. Actual pictures of the experimental setup are shown in Figures 2(a) and 2(b). The flue gas generator is a small combustion chamber fired with an oxy-fuel burner (Praxair J Burner). The chamber was made from a stainless steel (SS) pipe lined with refractory. The SS pipe is 8 inches in diameter and 27 inches in length. Inside the chamber, a 2-inch-thick refractory wall was cast as a heat insulation layer. Outside, the chamber was wrapped up with a blanket of 2-inch-thick fibrefrax and a thin layer of aluminum sheet to reduce heat loss from the chamber wall. On one end of the flue gas generator, a SS cover plate was welded. Two small ports were made on the plate to install a burner and a flame detector. The other end of the flue gas generator was reduced down to 2 inches in diameter to mate with the regenerator. In this study, a small jet burner (J burner) was used to combust natural gas due to its good flame stability feature. The J burner has a tube-in-tube structure. The center tube delivers natural gas and the outside tube delivers oxygen. An ultraviolet (UV) flame detector was placed with a 60 degree view angle to the J burner in order to monitor the flame stability. The flame detector lens was cooled by nitrogen to prevent overheating. In addition, the flame could be visually observed through a quartz view port attached to the sidewall of the chamber.

Under normal combustion conditions, the flue gas generator was operated at a slightly positive pressure of approximately 0.25 psig. Two overpressure protection devices were installed as a safety precaution. A 2-inch graphite rupture disk was mounted on top of the chamber to quickly release the furnace gases in case of a sudden pressure surge over 5 psig in the small furnace. A pressure switch with a threshold value set at 3 psig was connected to the end of the chamber. If the furnace is over pressurized, the pressure switch will be activated to de-energize the gas supplies to system. To ensure an accurate control on the gas flow rates, a mass flow meter was installed to adjust the flow rate of each gas stream. The flue gas temperature was measured with an R-type thermocouple at the exit of the chamber.

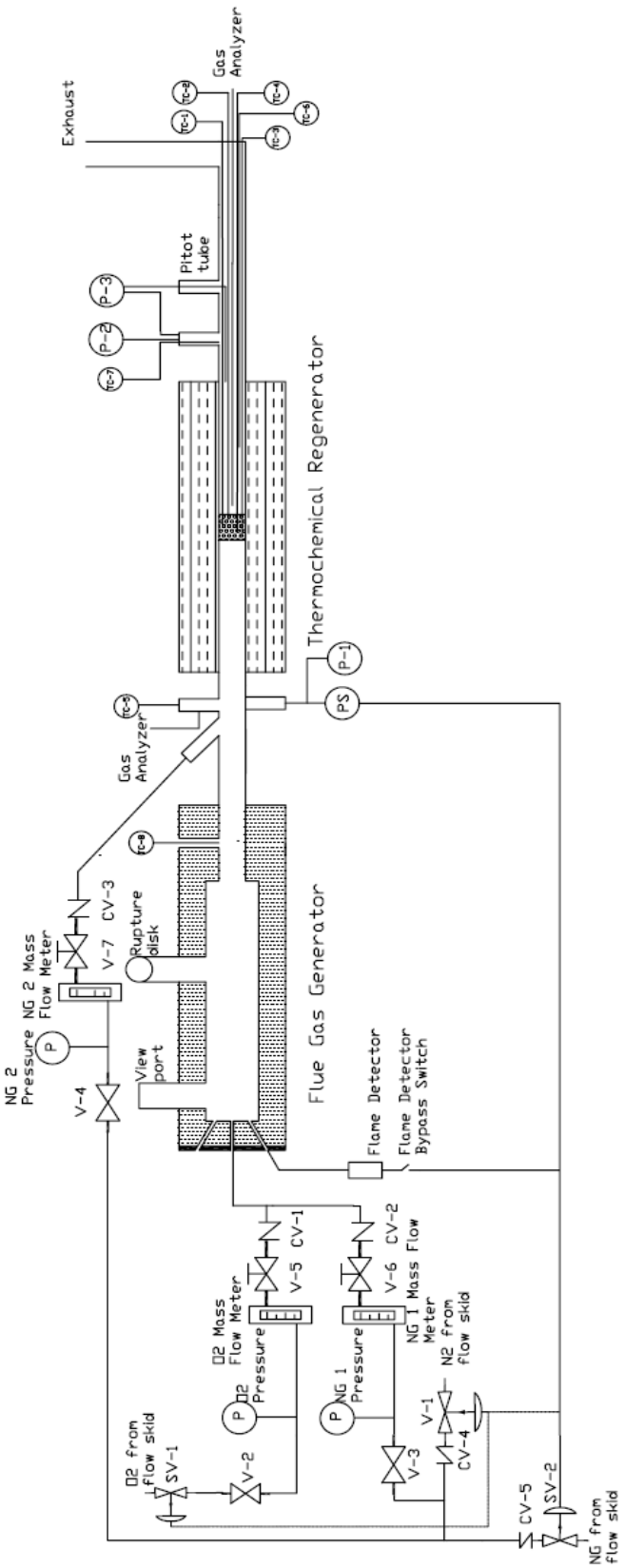

Figure 1. Bench-top test piping and instrumentation diagram

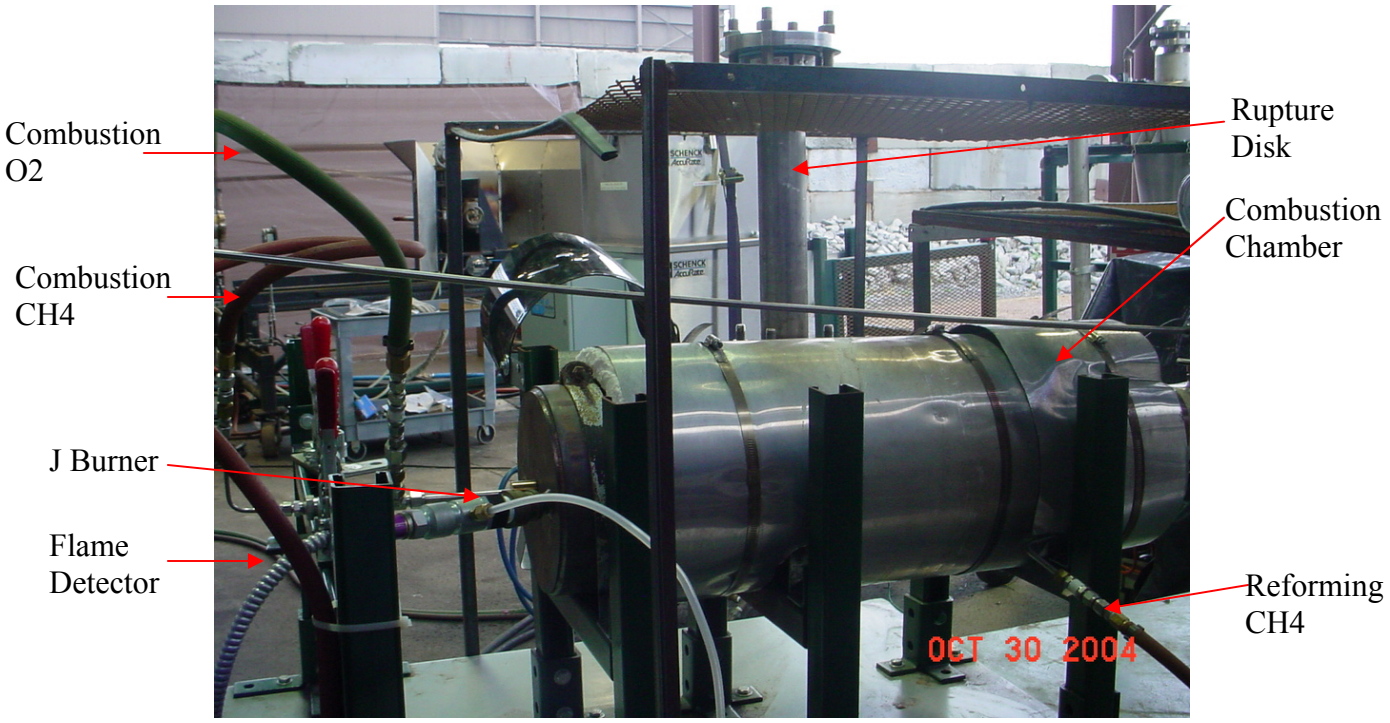

(a)

(b)

Figure 2. Bench-top test equipment (a) flue gas generator (b) thermo-chemical regenerator

Flue gas containing mostly CO_2 and steam, generated from natural gas and oxygen combustion, was transported downstream and blended with a second stream of natural gas. The mixture was well mixed before entering the simulated regenerator bed and then heated in the regenerator bed to promote the reforming reactions. The simulated regenerator bed was placed in a 1.3-inch diameter tubular reactor which is made from an alumina muffle tube and externally heated by an electrical heating element. A bed of alumina beads, as a heat storage/transfer medium, was sandwiched together with a pair of cordierite honeycombs on each end. The two honeycomb disks were pressed from both ends by a pair of smaller diameter alumina tubes, which fit inside of the alumina muffle tube, to ensure the alumina bed was packed tight and positioned at the center of the alumina muffle tube. The reforming reactants that were introduced into the muffle tube and heated, reacted as they passed through the honeycomb/alumina bed. The length of the bed was 8 inches. The thickness of the honeycomb disk was 0.5 inch each. The temperature of the electrically-heated muffle tube furnace was adjusted to control the reaction temperature. Four K-type thermocouples were installed into the alumina bed and spaced at an equal interval, to measure the temperature profile in the longitudinal direction. The alumina muffle tube was mated with the flue-gas generator by a stainless steel clamp and sealed up with fibrefrax threads. In the transition section between the flue gas generator and the muffle tube furnace, a sparger was installed at an angle of 45 degrees to the flue-gas pipe towards the alumina bed to inject the reforming natural gas. The sparger was made of a closed end quarter inch tubing with four arrays of 0.03125 inch diameter injection nozzles drilled on the tubing wall facing downstream. The reforming natural gas was injected parallel to the combustion flue gas stream. This design ensured good mixing of natural gas and flue gas. In addition, the stainless steel natural gas supply tubing was coiled on the combustion chamber of the flue gas generator. Therefore, extra heat from the flue gas generator preheated the reforming natural gas. The preheated temperature reached over 400 ºF. The exhaust end of the muffle-tube furnace was connected to an Inconel exhaust pipe. Exhaust gas was then sent to a stack and vented.

Product gas samples were drawn through an Eldwin condenser to remove moisture and then fed to a portable gas analytic system or a gas chromatograph (GC) for analysis. The portable analyzers had the capabilities of monitoring CO_2, CO, H_2, CH_4 and O_2 simultaneously. More

accurate dry product compositions were analyzed by a GC. The bench-scale test was a steady state experiment simulating the reforming step, i.e., the regenerator cooling period. Once a stable state was achieved, a product sample was analyzed. The temperature profile in the bed and the analyzer gas composition readings provided good indications to determine if the system was in a steady state.

Design of Experiments

In the bench-scale test, four variables were investigated: reforming reaction temperatures, residence times, and mixing ratios of flue gas to natural gas and bed materials. The reforming temperature was controlled by adjusting power input to the muffle tube furnace. As the reforming reactants passed through the bed, the bed temperature profile changed as indicated in Figure 3. Without the reforming natural gas flow, the two end thermocouples had lower temperature readings than the two in the middle due to the edge effects of the heating elements. After the reforming natural gas was injected, the reactants were preheated at the inlet, and then raised to a maximum temperature where most of the reforming reactions took place. Afterwards, the gas mixture temperature dropped due to endothermic reactions and also less heat available near the bed outlet. The maximum temperature in the bed was used as the process monitoring temperature. It had several levels ranging from 1800 ºF to 2300 ºF with each level 100 ºF apart. Due to the limit of the muffle-tube furnace heating capacity, bed temperatures of 2300 ºF or 2200 ºF were not achievable under some high gas flow rate test conditions.

The gas residence time was calculated by dividing the alumina-bed void volume by the gas volumetric flow rate. Since the bed length was fixed at 8 inches and was not easy to change, the reactant flow rates were changed in order to vary the residence time. Three levels were selected for the reactant flow rate: 48 SCFH (standard cubic feet per hour at 60 °F and 1 atm), 33 SCFH and 22 SCFH. The corresponding residence times were approximately 30 ms, 40 ms, and 60 ms for spherical packing materials. Under the ideal reforming reactions as shown in Equation (1) and (2), the mixing ratio of flue gas and natural gas of 1:1 is required to consume all the reactants and to generate CO and H_2. In this study, the mixing ratio of flue

gas to natural gas was selected at three levels as 1:1, 1:0.9 and 1:1.1. Three different bed materials were tested in the bench-scale test: 1/8 inch diameter alumina beads, 1/4 inch diameter alumina beads and cordierite honeycomb.

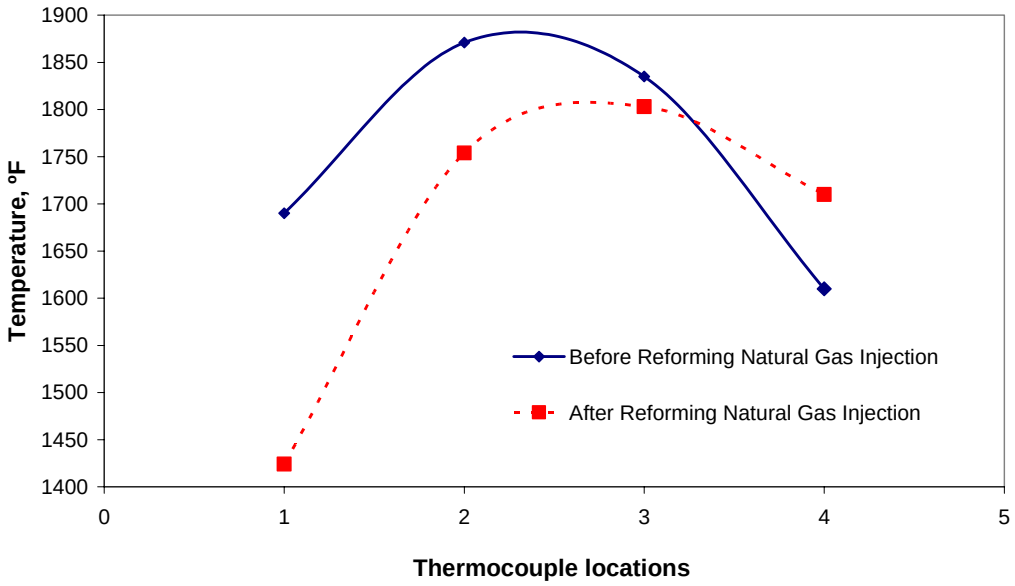

Figure 3. Regenerative bed temperature profile change before and after the reforming natural gas injection (reactant flow rate 22 SCFH, mixing ratio 1:1, 1/8-inch diameter alumina bead bed)

To start up the system and reach the test conditions, normally two operational steps were followed. The first step was the "combustion only" mode to warm up the entire system with a high natural gas-firing rate. J burner was ignited outside the flue gas generator and then inserted into the chamber after a stable flame was confirmed. The natural gas-firing rate was set at approximately 20 SCFH in the "warm up" combustion mode. In the mean time, the electrical heater of the muffle tube furnace was turned on to heat up the simulating thermochemical regenerator bed. The second step was a combination of the combustion and the reforming processes. When the temperature in the flue gas generator was raised up to 1200 ºF, the combustion firing rate was reduced to the designed rate. The reforming natural gas was blended into the flue gas and the regenerator bed temperature was controlled at a desired value. The system was held at the steady state in each operational condition for at

least ten minutes. During the holding period, the reforming product gas samples were collected and analyzed.

Results and Discussions

Temperature has an important impact on the reforming reactions. CO_2 and steam reforming reactions are both endothermic reactions. Higher temperatures lead to higher methane conversion ratios. Figure 4 shows the dry reforming product compositions measured by GC at different regenerator temperatures under the conditions of 22 SCFH total reactant flow rate, 1:1 mixing ratio and 1/8 inch diameter alumina beads for the regenerator bed. H_2 and CO contents increased as the temperature increased and CH_4 and CO_2 contents decreased with the increasing temperature. Data at other conditions had the same trend. The overall methane conversion ratio was calculated by assuming that there were only reactions of CO_2 and steam reforming reactions (Equation (1) and (2)) and that other side reactions were negligible. CH_4, CO and H_2 concentrations in the product measured from GC were applied to solve the methane reforming extent. From the hydrogen balance, the moisture content in the product was calculated. The relative error of this approach was approximately 10% which was acceptable for the complex reaction system. Two sources of errors were the assumption of no side reactions and the measurement errors derived from GC and mass flow meters.

Figure 5 shows the conversion ratio at different temperatures under the same operational conditions as Figure 4. As seen from both figures, methane conversion started at about 1800 ºF and increased sharply when the temperature was above 2000 ºF. Residence time also had strong influences on the reactions. Figure 6 illustrates H_2 concentrations at different residence times and different temperatures. The mixing ratio was 1:1 and the bed material was 1/8 inch diameter alumina bead. Under the same temperature, H_2 concentration increased as the residence time became longer. Under equilibrium conditions, H_2 concentration is supposed to be about 66% when the temperature is above 1800 ºF. Clearly the reactions were kinetically controlled and a longer residence time facilitated the reactions to reach the thermodynamic equilibrium. Among the curves of H_2 concentration with residence time at

different bed temperatures, it can be observed that the slope became sharper at a higher temperature due to higher reaction rate.

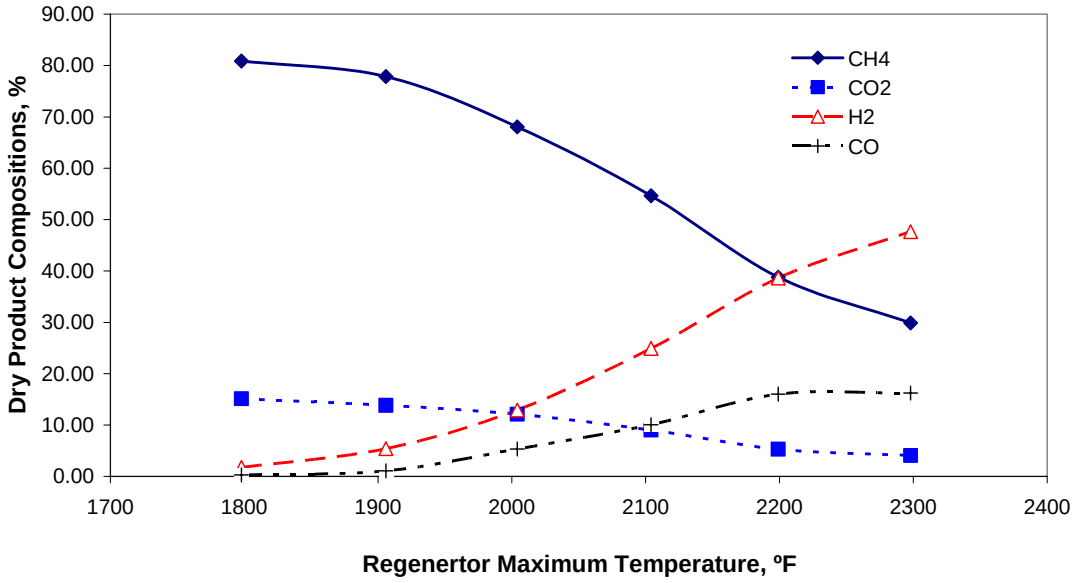

Figure 4. Dry product compositions at different temperatures (reactant flow rate 22 SCFH, mixing ratio 1:1, 1/8-inch diameter alumina bead bed)

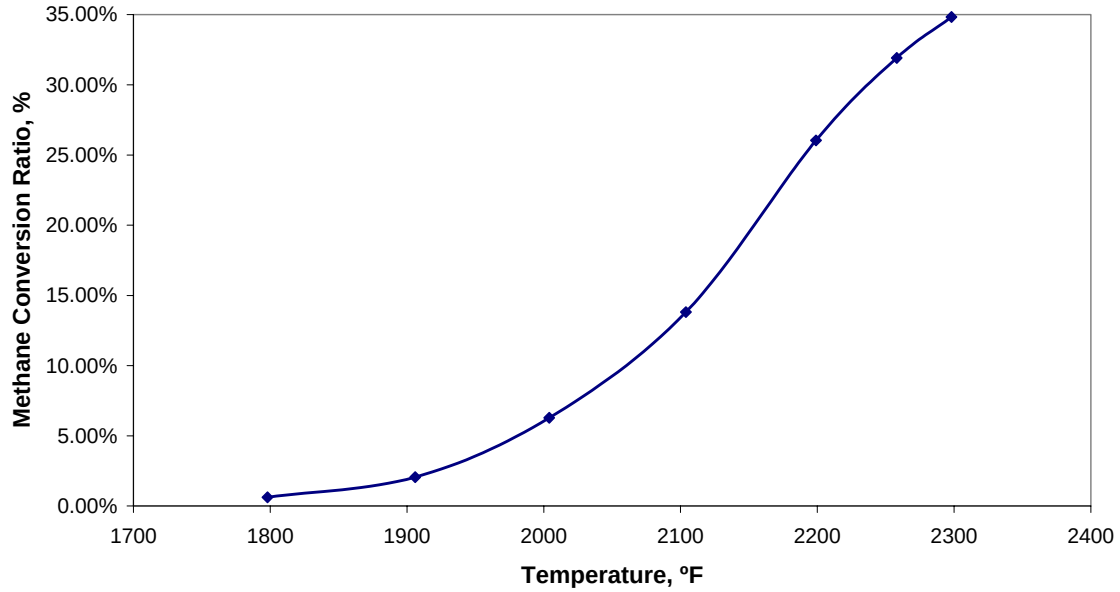

Figure 5. Methane conversion ratios at different temperatures (reactant flow rate 22 SCFH, mixing ratio 1:1, 1/8-inch diameter alumina bead bed)

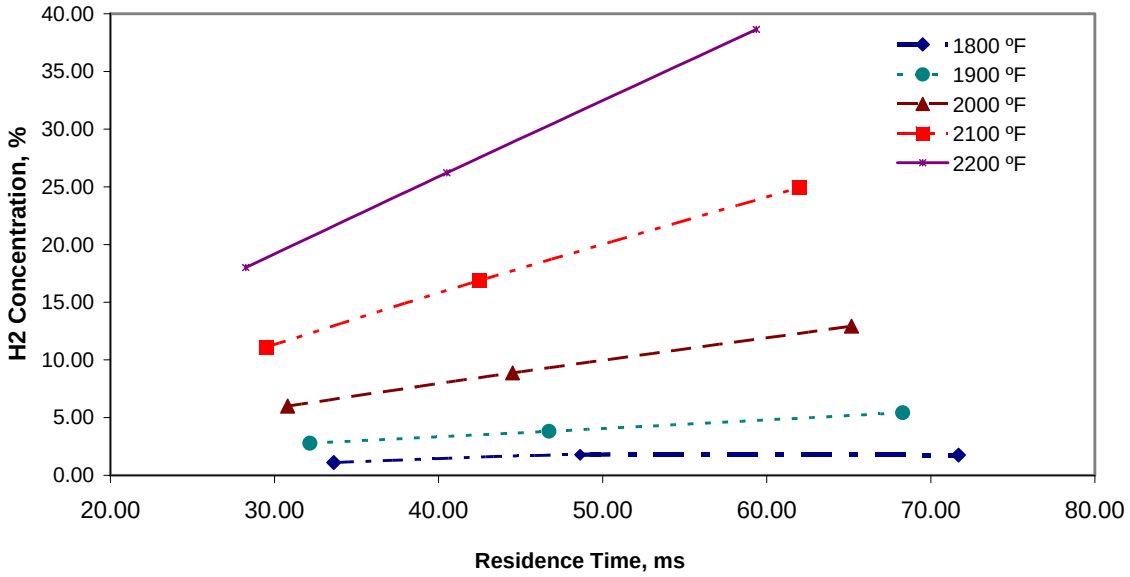

Figure 6. H_2 concentrations at different residence times (mixing ratio 1:1, 1/8-inch diameter alumina bead bed)

Figure 7 shows the effects of temperature on methane conversion at three different mixing ratios. The methane conversion ratio increased sharply with bed temperature, but the mixing ratio did not show a significant influence within the range of the experiment. The residence time was approximately 40 ms with the bed consisting of 1/8 inch diameter alumina beads. Similar results were obtained at other operational conditions. When the mixing ratio was changed, the combustion firing rate was held constant for the operational convenience, while the reforming natural gas flow rate was adjusted according to the designed mixing ratio. Therefore, there was a slight difference in the total reactant flow rate and the residence times for the different mixing ratios were somewhat different. As seen in Figure 7, the mixing ratio of 1:0.9 had somewhat higher conversion ratio which may be due to a longer residence time instead of the mixing ratio. In these experiments, the step change of the mixing ratio was not large enough to see a significant impact on methane conversion. More experiments are needed to determine the influences of this variable. Generally speaking, increasing the amount of one reactant should shift the reaction toward the product direction and promote the conversion of the reactants.

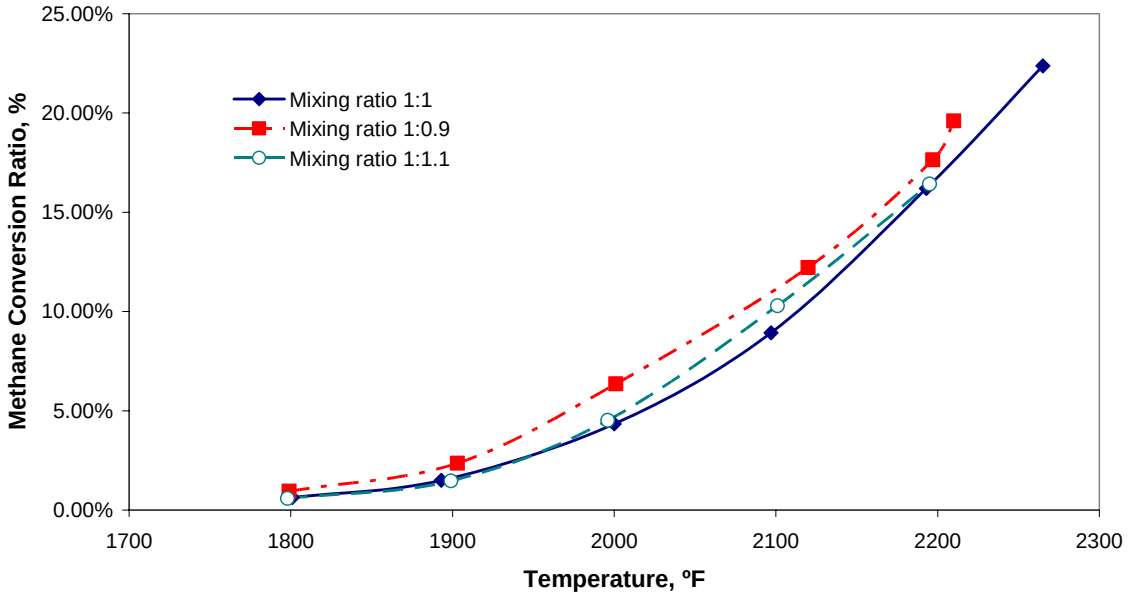

Figure 7. Methane conversion ratio at different mixing ratios (residence time is approximately 40 ms, 1/8-inch diameter alumina bead bed)

Figure 8 presents H_2 concentrations in different packing material beds when the mixing ratio was 1:1 and the reactant flow rate was approximately 22 SCFH. Different heat storage media or bed materials have different packing characteristics, i.e. specific surface area, thermal conductivity, and bed packing void fraction. The two alumina bead beds have the same material properties and similar void volume. However, the 1/8 inch diameter alumina beads have larger specific surface areas which enhance the heat transfer between solids and gases. As shown in the figure, 1/8 inch diameter beads exhibited a better performance over 1/4 inch diameter beads. Compared with 1/8 inch diameter alumina beads, cordierite honeycomb has a larger specific surface area and a larger void bed volume. Thus under the same reactant flow rate, the honeycomb packing provided a longer residence time and was expected to show a better performance. However, the H_2 concentration with the honeycomb was less than that of the 1/8 inch diameter alumina beads. The two potential causes for this surprising result are (1) differences in the bed temperature profile at the same peak temperature and (2) catalytic effects. Since the bed was heated electrically from outside the muffle tube, a radial temperature gradient developed with the gas mixture flowing in the axial direction. The

honeycomb provided more "radiation shields" in the radial direction due to the small cell structure, causing a cooler core temperature and a hotter outer temperature. Alumina is usually selected as the methane reforming catalyst support. Even though alumina beads were mainly used as the heat storage media here, some catalytic effects of alumina may result in higher methane conversion.

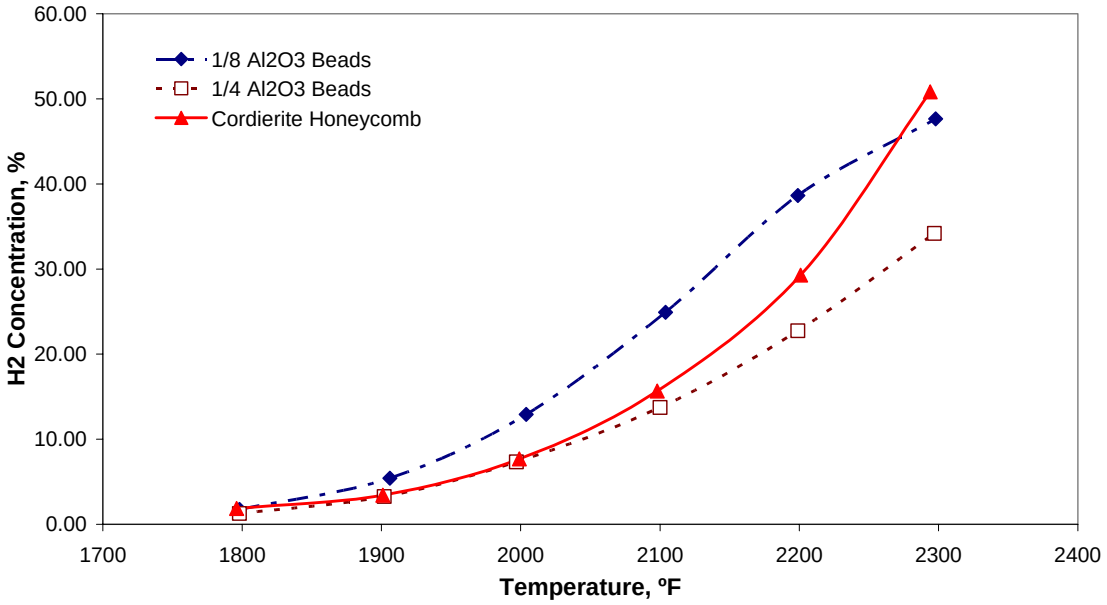

Figure 8. H_2 concentrations with different heat storage media (mixing ratio 1:1, reactant flow rate is approximately 22 SCFH)

Based on the data obtained from experiments, combustion products (i.e., CO_2 and H_2O) and natural gas reaction mechanism can be derived. The regenerator was similar as a plug flow reactor. The nature of methane reforming was complex involving many side reactions. The developed reaction mechanism mainly reflected CO_2 reforming and steam reforming and only represented the overall results instead of individual elemental reaction. One assumption made to simplify the kinetics was that the reaction rate was constant along the regenerator. Therefore, the reaction mechanism can be presented in the following format:

$$X_{CH_4} = k_0 \exp(-\frac{E_a}{T}) f_{CH_4,0}^{a} f_{CO_2,0}^{b} f_{H_2O,0}^{c} S_v \tau \qquad (3)$$

where X_{CH4} is CH_4 conversion rate. T is the regenerator maximum temperature with the unit in ºK. f_{CH4}, f_{CO2}, and f_{H2O} are the initial mole fractions of CH_4, CO_2 and H_2O in the reforming

reactants. S_v is the specific surface area of the reactor with the unit in $inch^{-1}$. τ is the residence time with the unit in ms. k_0, E_a, a, b and c are the parameters to be determined by curve fitting. Equation (3) was linearized and curve-fitted with the least square method. The result was shown in Equation (4):

$$X_{CH_4} = \exp(-118.81 - \frac{30770.42}{T}) f_{CH_4,0}^{-65.54} f_{CO_2,0}^{12.05} f_{H_2O,0}^{-93.02} S_v \tau \quad (4)$$

The R-squared value for the curve fitting was 0.95. The reaction mechanism can be used to predict the methane conversion ratio under conditions similar to the bench-top tests; for example, combustion product and natural gas mixing ratio 1:1, specific surface area 17-41 $inch^{-1}$, and residence time 30-80 ms.

There are two parts in the total absorbed heat, based on mass and heat balance calculations assuming that gas temperature had reached the maximum bed temperature measured by the bed thermocouples. Figure 9 shows the tests conducted at 22 SCFH reactant flow rate in 1/8-inch diameter alumina bead bed. The first one (the lower curve) was the sensible heat transferred to the reactants from the regenerator bed. The second one (the difference between the upper and lower curves) was the heat consumed by endothermic reactions. As the temperature increased, more reforming reaction took place resulting in higher reaction heat absorption fraction. In Figure 10, the total heat absorbed by reactant gases is plotted at different bed temperatures. The top three curves in the figure showed the results with the 1/8-inch diameter alumina beads at three different flow rates. Even though a lower flow rate gave a higher conversion ratio (due to a longer reactant residence time, as previously shown in Figure 6), a higher flow rate resulted in more heat absorption, since sensible heat was the dominant factor of the total absorbed heat in these test conditions. In Figure 10, the bottom two curves compared the results at the same flow rate for two different alumina bead sizes. Since the sensible heat portion was the same at the same temperature, the difference of these two curves represented the higher endothermic reaction heat absorbed in the 1/8-inch diameter alumina bead bed. In the thermo-chemical regenerator design, both heat absorption modes need to be considered to maximize the total heat recovery capability.

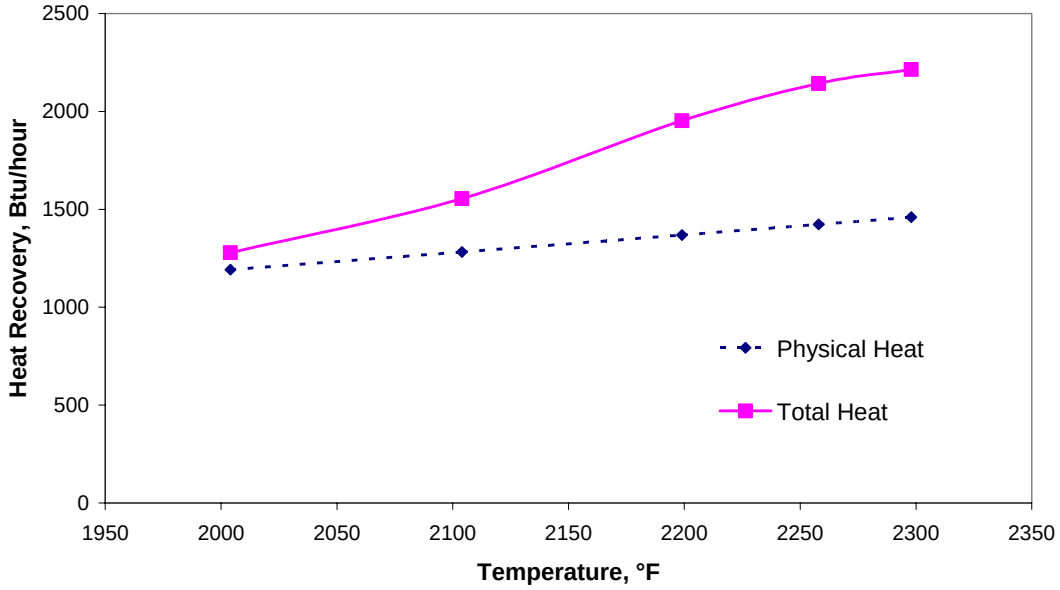

Figure 9. Heat recovery at different temperatures (1/8-inch diameter alumina bead bed, 1:1 mixing ratio, reactant flow rate is approximately 22 SCFH)

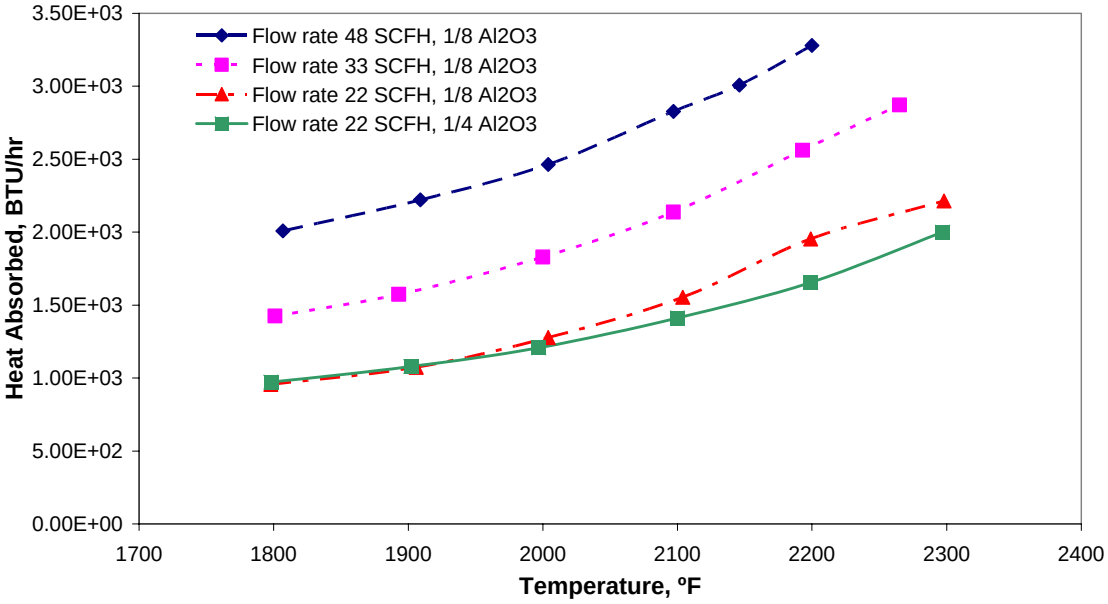

Figure 10. Heat absorbed by reactant gases

Summary

In the bench-scale test study, the effects on reforming reactions of regenerator temperatures, residence time, mixing ratio of flue gas to methane, and bed materials were investigated. The highest methane conversion achieved was about 35% at the conditions of 2300 ºF peak bed temperature, 60 ms residence time, and 1:1 mixing ratio with the bed of 1/8-inch diameter alumina beads. The dry product compositions were 47.5% H_2, 16.2% CO, 29.9% CH_4 and 4.1% CO_2. The heat absorbed by the reforming gas mixture from the bed at the natural gas flow rate of 11 SCFH was approximately 2210 Btu/hour, consisting of 1460 Btu/hour of sensible heat and 750 Btu/hour of reaction heat. This steady-state study demonstrated the feasibility of the thermochemical regenerator concept and provided useful data to design a pilot-scale system.

3. PILOT SCALE REGENERATOR TESTS

A pilot-scale regenerator system was built to test the feasibility of both the regenerative oxygen preheating and the regenerative thermochemical heat recovery concepts. The characteristics of the pilot-scale system were initially tested thoroughly by preheating nitrogen in order to ensure the safe operation of the test equipment prior to oxygen and reforming tests.

3.1 TESTS WITH NITROGEN

Experimental Setup

Thermal regenerators consist of at least two heat storage beds and transfer heat between two fluids. Hot fluid (i.e., furnace flue gas) and cold fluid (i.e. oxygen or fuel) pass through each alternately. Heat from the hot gas is temporarily stored in a permeable heat storage media. This thermal energy is then transferred to the cold gas in a subsequent step. Usually the regenerators have countercurrent flows. During the bed heating period, all the surface areas of the regenerator heat storage media are immersed in the hot gas and the sensible heat is retained in the bed. At the end of the period, the hot gas is switched off and the cold gas starts to flow through the same channels over the heated surface area. The thermal energy is recovered by the cold gas during the cold period at the end of which another cycle of bed heating starts. The switching of the two fluids and the timing of each period can be controlled by solenoid valves. During the reversal at the end of each period, the residual gas in the bed would partially mix with the incoming gas in the next period and is either injected into or exhausted out of the furnace. The result would be a loss of oxygen in the oxygen preheating mode and a loss of fuel in the fuel reforming mode. It also raises a concern on combustion of residual oxygen and fuel under some conditions. A purge step, using the recycled flue gas, is designed in the proposed system. In this experiment, the hot fluid was the flue gas in the furnace generated from an oxy-fuel burner. The cold fluid was nitrogen. A nitrogen purge period was added at the end of the hot period and the cold period to simulate the purge step with recycled flue gas.

The experimental setup using a two-bed system is shown schematically in Figure 11. Actual pictures are shown in Figure 12. The regenerator beds consisted of cast refractory shells and packed beds with 3 1/2-inch in diameter and 5 5/8-inch in length which were filled with 1/8 inch diameter alumina beads. The beads were held in place by a piece of 1/4 inch thick cordierite honeycomb at the hot furnace end and a piece of metal wire mesh at the cold end. Three thermocouples were embedded in the regenerator bed in order to monitor the temperature profile along the regenerative bed; TC #1 at the front face of the bed hot end, TC #2 in the middle, and TC #3 at the back face of the bed cold end. The regenerator beds were mounted to the burner end wall of the furnace and connected to the open refractory ports in the furnace end wall.

As indicated in Figure 12 (a), the furnace gas was alternatively exhausted through the regenerators by two eductors driven by high pressure air. Each eductor was installed with a globe valve to adjust the air flow rate. Thus vacuum was created at the inlet of the eductor which controlled the exhaust gas flow rate. The exhaust gas temperature was monitored by a K-type thermocouple and the flow rate was measured by the nozzle flow meter installed at the upstream of the eductor. As shown in Figure 12 (b), each regenerator was mounted on the furnace by a flange. The cold end was connected to a brass cross which communicated with three gas pipes. One branch was for the exhaust gas delivery which was hooked up with the eductor. The second one was connected with nitrogen purge gas. The third one provided the nitrogen preheating gas supply. Three solenoid valves were also installed near the cross to switch the gases on and off through the regenerator. Nitrogen was supplied from the furnace flow skid which had a supply pressure of approximately 100 psig. After the purge gas or the preheating gas solenoid valve closed, pressure was built up in the supply pipe, equal to the supply pressure. When the solenoid valve opened, the pressure released from the supply pipe to the regenerator. When the solenoid valves were turned on and off, the furnace experienced pressure upsets. To minimize the pressure surges, critical orifice plates were mounted next to the solenoid valves. The critical orifices restricted the passing gas velocity and dramatically reduced the pressure surges. However, the critical orifices limited the flexibility to change the gas flow rate. To adjust the volumetric flow rate, the critical orifice size had to be changed. The timing of the switching valves was controlled by a Modicon control panel.

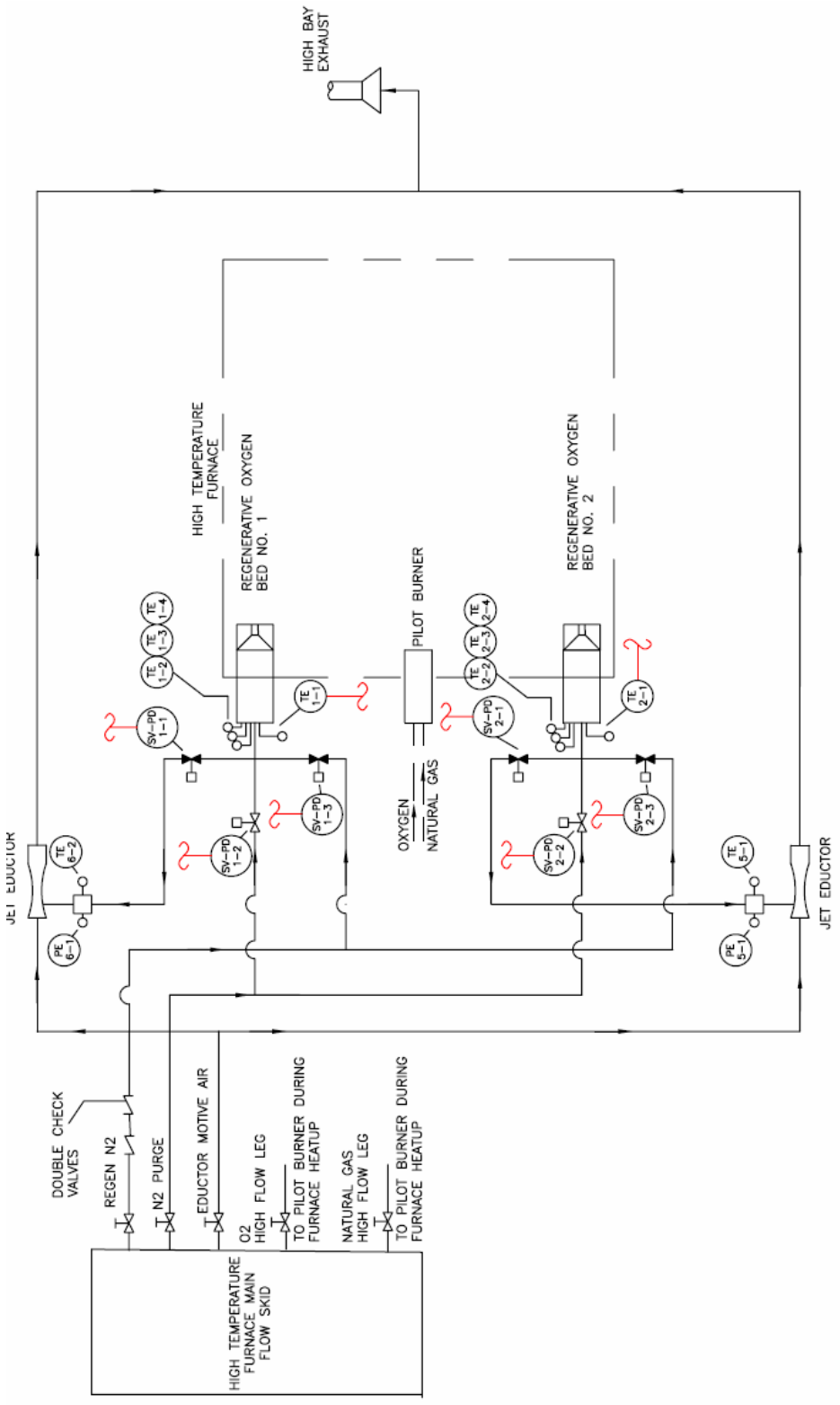

Figure 11. Two-bed N_2 regenerator system piping and instrumentation diagram

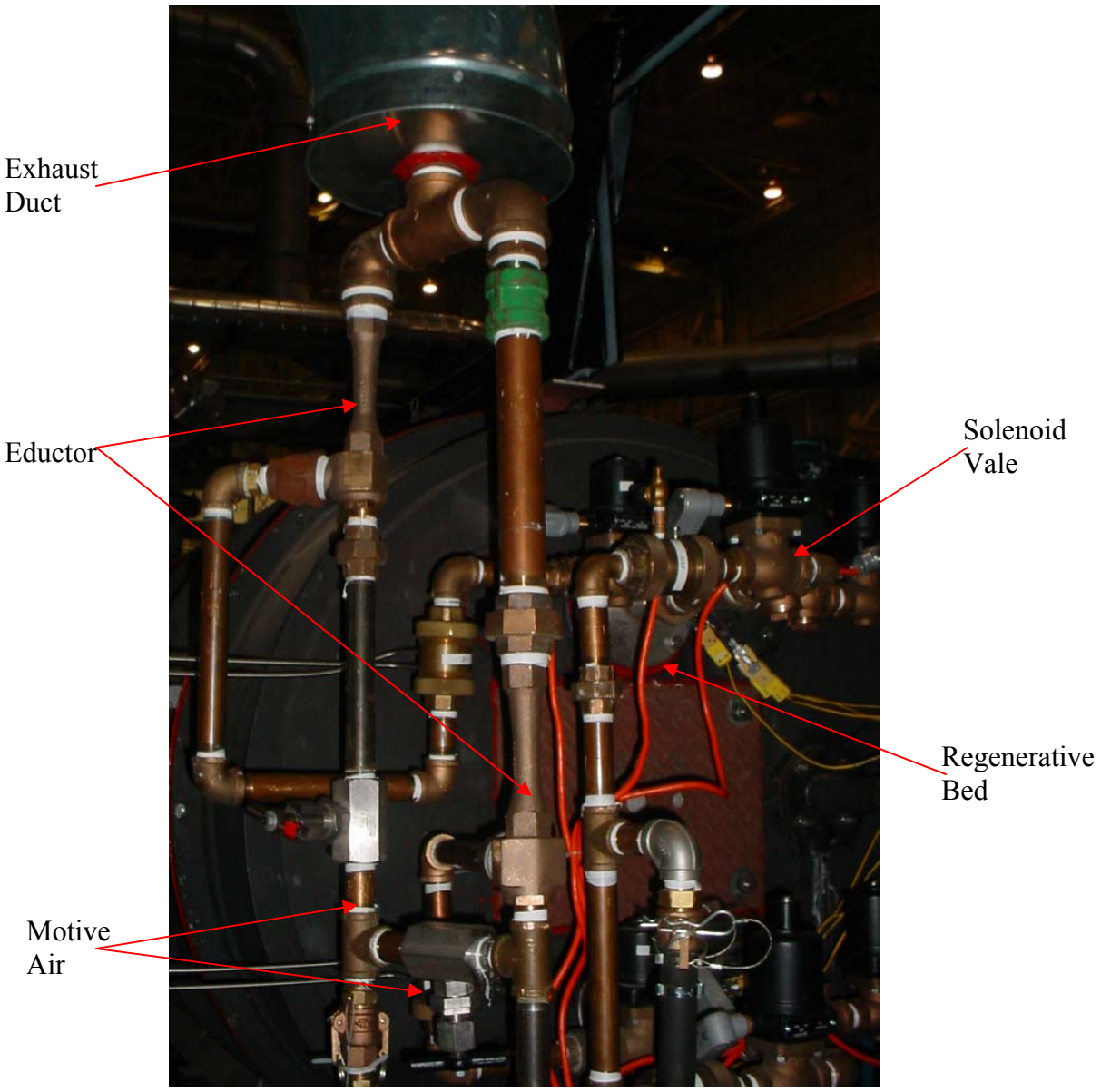
Exhaust
Duct
Eductor
Solenoid
Vale
Regenerative
Bed
Motive
Air

(a)

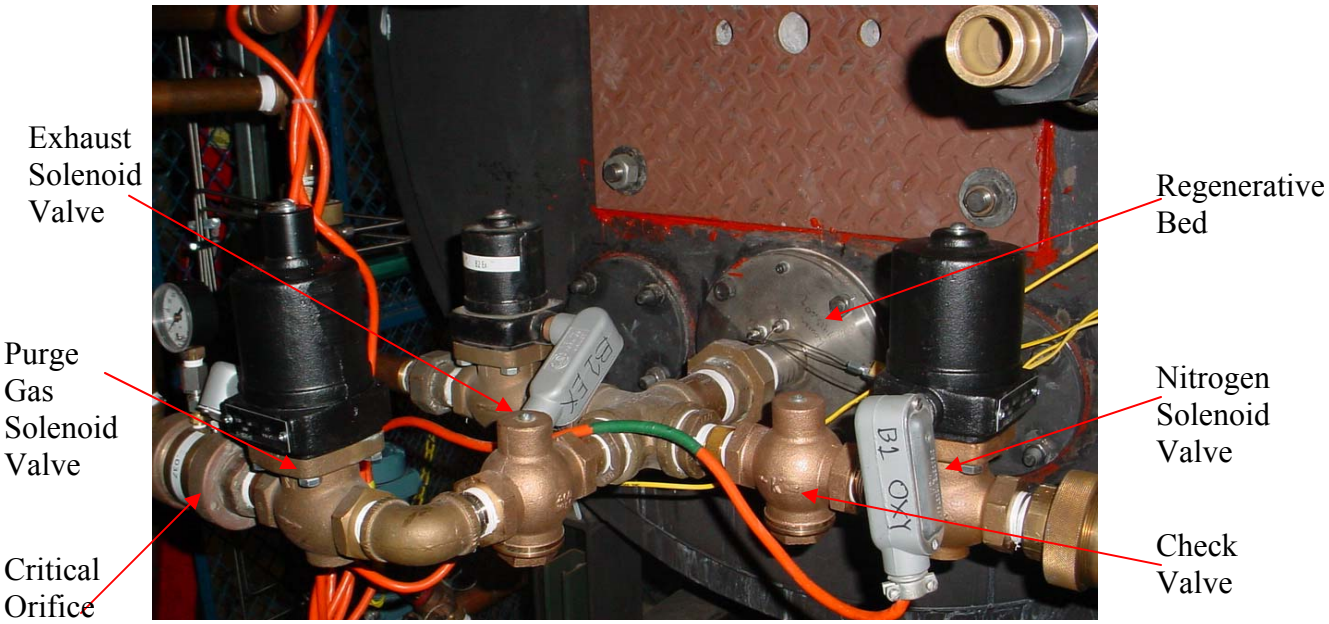

(b)

Figure 12. Nitrogen preheating two-bed regenerator system (a) regenerator exhausts system (b) regenerator switching valve system

Design of Experiments

Two variables were investigated in the experiments: the switching valve timing and the flow rate ratio between the exhaust gas and the preheating gas. Because the regenerators were initially designed for a four-bed system instead of a two-bed system, the ratio of the hot period to the cold period was set to approximately 3:1. For example, the cold periods were 10s, 15s, 20s and 25s; the corresponding hot periods were 28s, 43s, 58s and 73s. There was a one-second purge period following each hot or cold period. The nitrogen purge gas flow rate was set at 200 SCFH in all the cases. The exhaust gas flow rate was controlled at approximately 355 SCFH. The preheating nitrogen was selected at three different flow rates: 1000 SCFH, 750 SCFH, and 500 SCFH.

Results and Discussions

The furnace was heated up to approximately 2400 °F by using a pilot burner. The regenerators were then started. As shown in Figure 13, temperatures in the regenerator started cycling as well. TC #1 is the temperature at the hot end (or the exhaust inlet) of the

regenerator; TC #2 is the temperature in the middle of the regenerator; TC #3 is the temperature at the cold end (or exhaust outlet) of the regenerator. As the exhaust cycle started, the regenerator temperatures began to increase due to the heat transfer from the hot flue gas to the bed. All three temperatures reached high-peak values at the end of the exhaust cycle. Following the exhaust cycle, the regenerator underwent a post-exhaust purge cycle, a nitrogen preheating cycle and a post-preheating purge cycle. In these three cycles, cold nitrogen passed through the heated regenerator and carried heat back to the furnace. The regenerator temperatures began to drop and reached lowest values at the end of the post-preheating purge cycle. The cyclic temperature profile reached a repeatable pattern after a few initial cycles, which indicated that the regenerator operation achieved a steady state. The regenerative cycle shown in Figure 13 consisted of 73s exhaust, 1s purge, 25s nitrogen preheating and 1s purge. The exhaust gas, the purge nitrogen and the preheating nitrogen flow rates were 359 SCFH, 200 SCFH, and 1000 SCFH, respectively. The hot-end high peak temperature reached 2282 °F and the lowest temperature was 2028 °F. The temperature swing at the hot end was approximately 254 °F and the average temperature was 2155 °F. The cold-end high-peak temperature was 648 °F and the lowest temperature was 246 °F. The swing was 402 °F and the average was 447 °F.

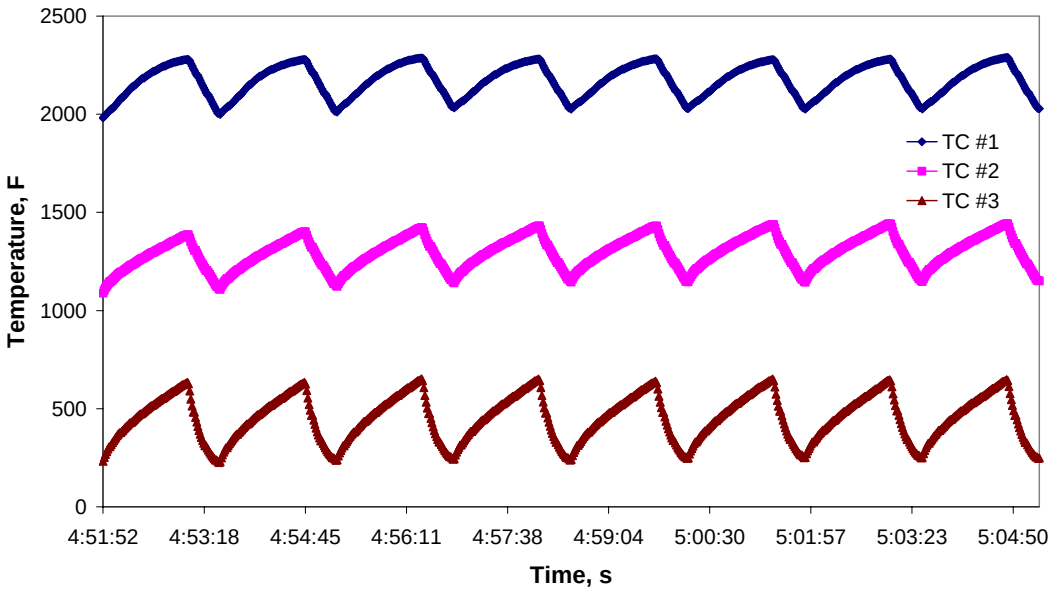

Figure 13. Temperature profile in the regenerator for nitrogen preheating

Figure 14 presents the temperature variations vs. the nitrogen purge cycle times. The flow rates of exhaust gas, nitrogen purge and preheating nitrogen were kept at about 375 SCFH, 200 SCFH and 1000 SCFH, respectively. Seven R-type thermocouples were mounted along the furnace. The furnace gas temperature in the figure was assumed to be the temperature reading from the thermocouple located closest to the burner end. As shown in Figure 14, the furnace gas temperature was maintained at 2400 °F. The average temperatures at both the hot and the cold ends increased and the band of the temperature swing expanded as the cycle time became longer. Although the temperature swing was expected to expand with increasing cycle times, the increase in the temperature swing was much smaller at the hot end than that in the cold end. This represents the bed condition that the capacity rate ratio, C_c/C_h, was less than 1 and most of the heat exchange within the bed was taking place in the colder half of the bed. C_c and C_h are the products of fluid flow rate and its specific heats for cold fluid and hot fluid respectively,

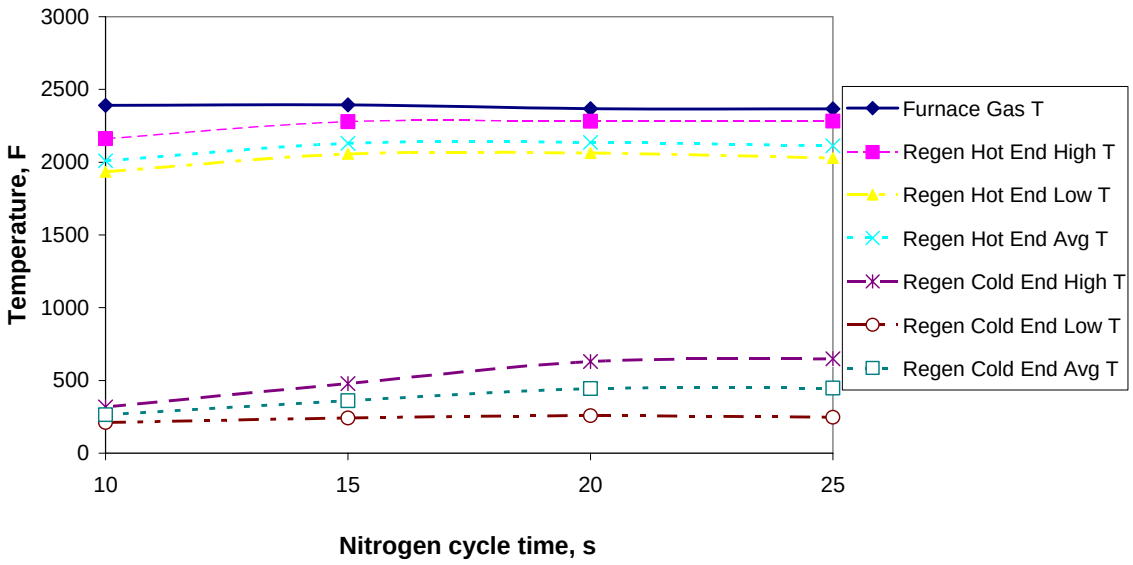

Figure 14. Nitrogen cycle time impacts on the regenerator temperature profile

The average cold-end temperature increased from about 250 ^{o}F at the nitrogen preheating cycle time of 10 second to about 450 ^{o}F at 25 seconds, indicating a significant decrease in the heat recovery by the regenerator. It was attributable, in part, due to an increase in the ratio of

the exhaust gas flow to the total cold nitrogen flow in a cycle, since the purge nitrogen cycle was kept at 1 s. At the nitrogen preheating cycle time of 10 second, the exhaust gas flow and the total cold nitrogen flow per a complete regenerator cycle, (including the nitrogen purge flow,), were 2.92 SCF and 2.89 SCF respectively, which gave an exhaust gas to nitrogen flow ratio of 1.01. When the nitrogen preheating cycle time was increased to 25 second, the exhaust gas flow and the total cold nitrogen flow per a complete regenerator cycle, including the nitrogen purge flow, were 7.60 SCF and 7.05 SCF respectively, which gave an exhaust gas to nitrogen flow ratio of 1.08. In a practical system, the effects of the finite reversal time and the purge flow requirement, as well as the reliability, of valves must be considered to select the optimum cycle time.

Another variable investigated was the preheating nitrogen flow rate. The exhaust gas and purge gas flow rates were controlled at 355 SCFH and 200 SCFH, respectively. The preheating nitrogen flow rate was varied at three levels: 1000 SCFH, 750 SCFH and 500 SCFH. Figure 15 illustrates the data for 15s nitrogen preheating cycle case. As more nitrogen gas passed through the regenerator, the capacity ratio of the cold-fluid-to-the–hot-fluid increased and the average temperature of the regenerator dropped.

The amount of heat transferred per regenerator cycle was estimated from the gas flow rates and the measured bed temperatures before and after each flow cycle by the following three equations:

$$Q_h = \rho_h \cdot C_{p,h} \cdot V_h \cdot (\overline{T_{i,h}} - \overline{T_{o,h}}) \cdot t_h \tag{5}$$

$$Q_m = m \cdot C_{p,m} \cdot (\overline{T_{h,avg}} - \overline{T_{c,avg}}) \tag{6}$$

$$Q_c = \rho_c \cdot C_{p,c} \cdot V_c \cdot (\overline{T_{o,c}} - \overline{T_{i,c}}) \cdot t_c \tag{7}$$

where Q_h, Q_m, and Q_c are the heat released by the hot fluid, the heat retained in the bed the heat recovered by the cold fluid. C_p, ρ, V, t, $\overline{T_i}$, $\overline{T_o}$ are the heat capacity, density, volumetric flow rate, cycle time, gas average inlet and outlet temperatures. The mass of the bed is m. Subscripts h, m, and c denote the hot fluid, the bed and the cold fluid, respectively. $\overline{T_{h,avg}}$ and $\overline{T_{c,avg}}$ are the average heat storage media temperatures during the heating and cooling cycles.

When the regenerator reaches the steady cycle, the conditions $Q_h = Q_m = Q_c$ are met for an ideal regenerator without radiative heat fluxes and wall-heat losses.

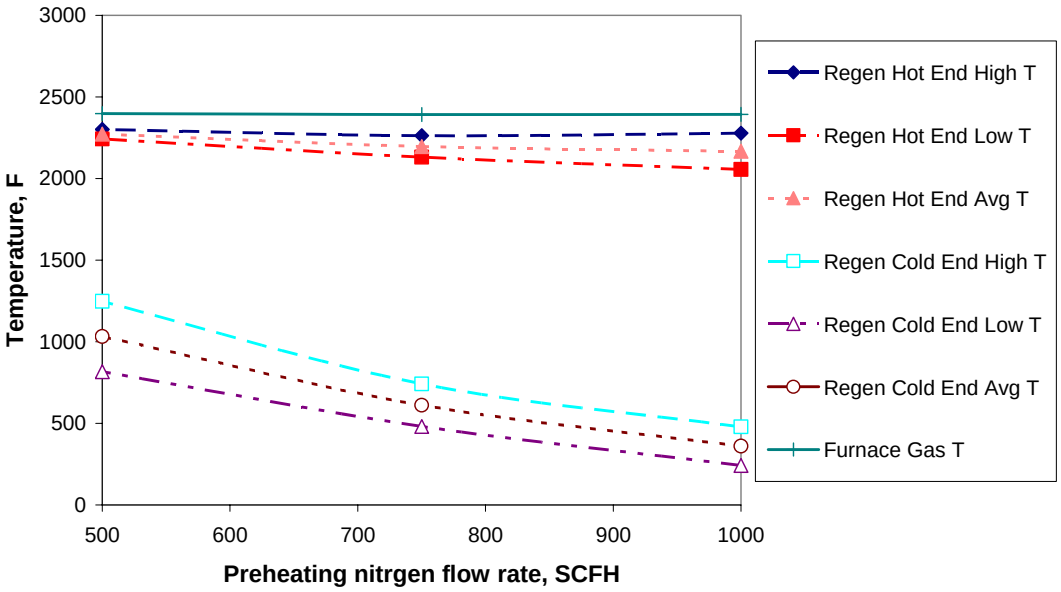

Figure 15. Preheating nitrogen flow rate impacts on the regenerator temperature profile

The average heat exchange rate, the average exhaust gas flow rate and the average nitrogen flow rate in one hour per bed were calculated by multiplying the number of the cycles in one hour to the heat stored in each cycle, to the actual exhaust gas flow rate in each cycle, and to the actual nitrogen flow rate in each cycle, respectively. The heat balance around the regenerator bed itself was checked using the hot-end thermocouple TC #1 and the cold end thermocouple TC #3 as these thermocouple readings were considered to be reasonably close to the local gas temperatures. The results of heat balance calculations were reasonably good when TC # 3 was less than 200^{o}F, but underestimated the heat recovered by nitrogen substantially when TC #3 was hotter. For the total amount of the heat transferred per cycle, the heat exchanges in the hot-end honeycomb and in the cold-end pipings had to be included. For the flue gas temperature entering the regenerator port, the furnace thermocouple closest to the regenerator was used. For the flue gas temperature leaving the regenerator, the average of TC #3 and the thermocouple readings at the downstream flow meter was used. Thus the heat exchange rate reported in this study is defined as “the heat released by the hot flue gas

through the regenerators" and includes natural heat losses from the regenerator walls. The actual heat recovered by the nitrogen flow was less than the heat exchange rate

Figure 16 shows the average heat exchange rate in one hour per single bed vs. the average nitrogen flow rate in one hour under different cycle times. The heat exchange rate per bed increased linearly with the average nitrogen flow rate and changed little with the cycle time. The bed temperature decreased with increasing nitrogen flow, but the hot-end temperature (TC #1) stayed above 2000 F in most cases. The maximum heat exchange rate under the test conditions was about 15,000 Btu/hr. These results indicate that the average heat exchange rate was limited by the amount of the average nitrogen flow rate used during the tests and that the maximum heat exchange capacity of the pilot-scale bed is significantly greater. As discussed further on, gross heat exchange rates over 19,000 Btu/hr were observed under some natural gas reforming tests.

In order to evaluate the effectiveness of the regenerator, thermal ratio, η, as defined by Equation (8), was calculated for different cycle times and different preheating nitrogen flow rates and plotted in Figure 17.

$$\eta_{N_2} = \frac{T_{h,i} - T_{h,o}}{T_{h,i} - T_{c,i}} \tag{8}$$

$T_{h,i}$ is the hot gas (exhaust gas) inlet temperature. The furnace gas temperature is applied as $T_{h,i}$. $T_{h,o}$ is the hot gas outlet temperature which is the regenerator average outlet temperature. $T_{c,i}$ is the cold gas (nitrogen) inlet temperature. Here, the 77 °F room temperature was selected as $T_{c,i}$. Thermal ratio, η, is a measure of the effectiveness of a heat exchanger in the hot-gas side and it becomes 1 under the ideal condition, i.e., when the hot exhaust gas leaves the regenerator at the same temperature as the cold gas inlet temperature. The maximum attainable value of η depends on the capacity rate ratio, C_c/C_h, where C_c and C_h are the product of the fluid flow rate and its specific heat for cold fluid and hot fluid respectively.

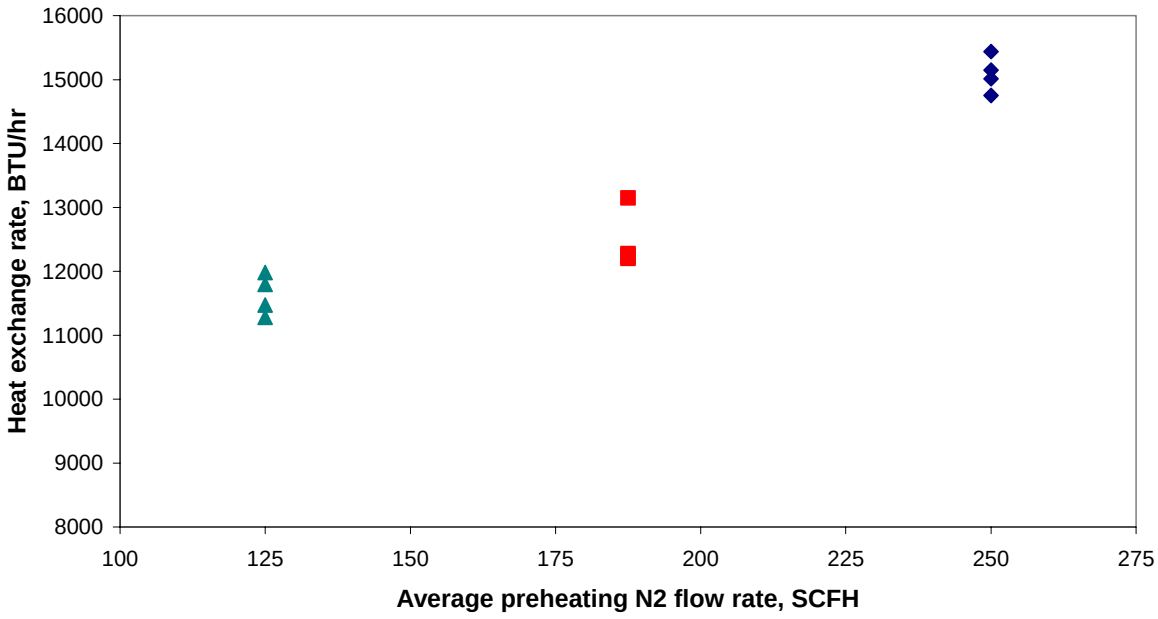

Figure 16. N_2 preheating heat exchange rate at different N_2 flow rates

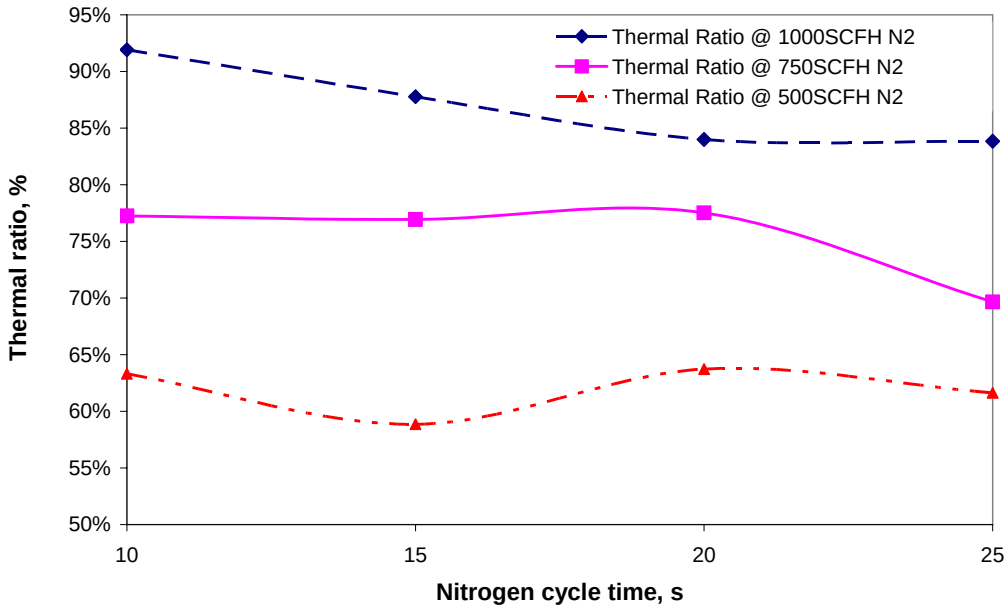

Figure 17. Thermal ratio at different cycle times and nitrogen flow rates

Figure 17 shows thermal ratios vs. nitrogen cycle time for three different nitrogen flow rates. Thermal ratio increased as the actual nitrogen flow rate was increased, i.e., about 50-64% at 500 SCFH, about 70-75% at 750 SCFH, and 84-92% at 1000 SCFH. With increased cold gas flow rates, more heat was transferred from the bed to nitrogen and the temperature of the regenerator bed became lower, resulting in better thermal ratios. In the practical operation of regenerators, the exhaust gas temperature after the regenerator is controlled below a certain limit, say 400 F, in order to protect the piping components and to maintain a good heat recovery efficiency. Thus thermal ratios over 80% are typical in practical regenerator operation.

In order to predict regenerator performances under different flow conditions, an empirical regenerator heat transfer model, known as the Λ-Π model, was applied here [8]. Λ refers to the reduced length and Π refers to the reduced period. They are calculated by the following equations for the hot gas exhaust period:

$$\Lambda_h = \frac{h_h A}{\dot{m}_h C_{p,h}} \tag{9}$$

$$\Pi_h = \frac{h_h A \tau_h}{S_{fr} L(1-\varepsilon)\rho_m C_{p,m}} \tag{10}$$

Where h_h is the heat transfer coefficient of the hot gas, A is the heat transfer surface area, $\dot{m}_h$ is the hot gas mass flow rate, $C_{p,h}$ is the hot gas heat transfer capacity, τ_h is the heating period, S_{fr} is the frontal area of the regenerator bed, L is the length of the bed, and ε is the void fraction of the bed, ρ_m is the density of the regenerator heat storage media, and $C_{p,m}$ is the heat capacity of the heat storage media. Λ and Π in the cold, i.e., preheating, period can be calculated in the same way. The correlations between thermal ratios and Λ-Π are listed in a table in Reference 8. With the derived thermal ratios, the hot fluid and the cold fluid outlet temperatures can be calculated using Equation (11) and (12):

$$\eta_h = \frac{T_{h,h} - T_{c,h}}{T_{h,h} - T_{c,l}} \tag{11}$$

$$\eta_c = \frac{T_{h,l} - T_{c,l}}{T_{h,h} - T_{c,l}} \tag{12}$$

Where η_h and η_c are the thermal ratios of the hot and cold periods, respectively, $T_{h,h}$ is the bed hot end high peak temperature, $T_{c,h}$ is the bed cold end high peak temperature, $T_{c,l}$ is the cold end low peak temperature, $T_{h,l}$ is the hot end low peak temperature. η_h and η_c are different from η_{N2}. η_{N2} reflects the overall regenerator heat transfer performance with the control volume containing the entire bed. η_h and η_c only represent their own periods with the control volume between the hot end and the cold end thermocouples. The hot-and cold-end temperatures in the regenerative bed can be estimated by the Λ-Π model.

Figure 18 shows a comparison of the measured temperatures and the predicted temperatures at different cycle times when the exhaust gas flow rate was about 375 SCFH and the preheating N_2 flow rate was 1000 SCFH. The relative error was approximately 13% at the hot end and approximately 23% at the cold end. The discrepancy may come in part from gas physical properties in Equation (9) and (10). Although the gas properties vary with temperature, constant properties at the average bed temperature were applied in Equation (9) and (10). The main source of error may be the accuracy of the correlations of thermal ratios and Λ-Π for different regenerator systems. As an empirical approach, the Λ-Π model provides a simplified methodology to predict the regenerative bed temperature profile at a reasonable accuracy.

Summary

The physical heat transfer characteristics of the regenerators were investigated using nitrogen. After the initial warm-up period, the regenerator temperature produced a regular cyclic pattern as the hot and cold gases were alternately introduced. Nitrogen preheat temperature above 2000 °F was obtained at the furnace temperature of 2400 ºF. The average heat exchange rate increased linearly with the nitrogen flow rate and heat exchange rates of about 15,000 Btu/hr were achieved at the average nitrogen flow rate of 250 SCFH. The cycle time did not have a strong impact on the bed temperature profile. The observed bed temperature profiles were in reasonable agreement with those predicted by the Λ-Π heat transfer model.

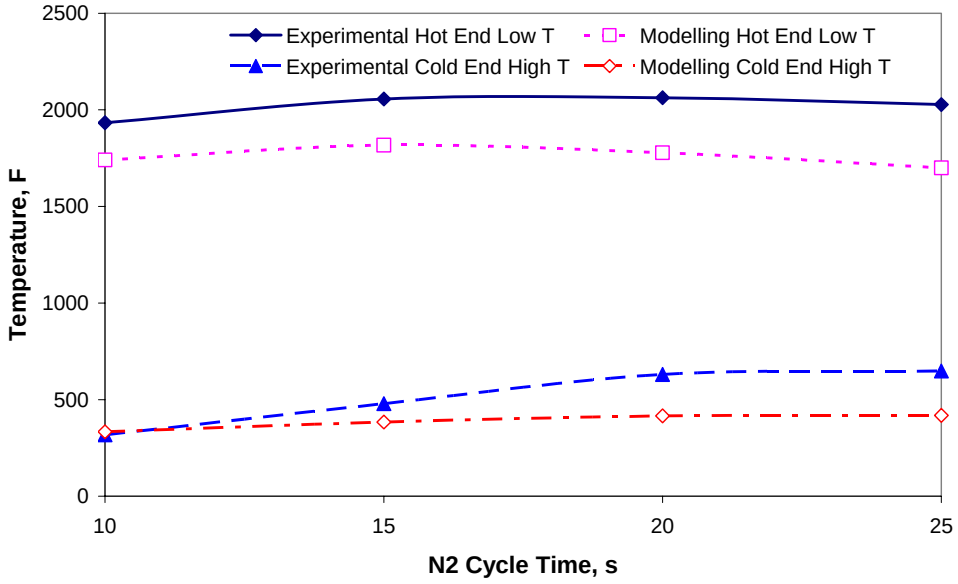

Figure 18. Temperature comparison of experiments and Λ-Π models for N_2 preheating

3.2 OXYGEN PREHEATING TEST

Experimental Setup

The experimental setup for oxygen preheating was basically the same as that of nitrogen tests and shown in Figure 11 and 12. All of the oxygen piping materials were selected and cleaned for oxygen service. The purge gas was nitrogen as previously indicated.

Design of Experiments

Oxygen preheating was tested with a four-bed regenerator system and a two-bed regenerator system. The cycle time ratios of the exhaust cycle to the oxygen cycle were designed to be 3:1 in the four-bed system and 1:1 in the two-bed system. The actual cycle times selected for the four-bed system were:

(1) 10s O_2 / 1s purge /28s exhaust / 1s purge,

(2) 15s O_2 / 1s purge / 43s exhaust / 1s purge,

(3) 20s O_2 / 1s purge / 58s exhaust / 1s purge, and

(4) 25s O_2 / 1s purge / 73s exhaust / 1s purge.

For the two-bed system they were:

(1) 10s O_2 / 1s purge / 8s exhaust / 1s purge,
(2) 15s O_2 / 1s purge / 13s exhaust / 1s purge,
(3) 20s O_2 / 1s purge / 18s exhaust / 1s purge, and
(4) 25s O_2 / 1s purge / 23s exhaust / 1s purge.

Three different oxygen flow rates were selected for the four-bed system and also for the two-bed system. The exhaust gas flow rate was adjusted according to the oxygen flow rate selected to maintain reasonably low, cold-end temperatures. For the four-bed system, the three flow rate levels selected were 200 SCFH exhaust / 630 SCFH O_2, 280 SCFH exhaust / 1010 SCFH O_2, and 320 SCFH exhaust / 1200 SCFH O_2. For the two-bed system, they were 200 SCFH exhaust / 230 SCFH O_2, 280 SCFH exhaust / 350 SCFH O_2, and 340 SCFH exhaust / 470 SCFH O_2.

Results and Discussions

As was the case for nitrogen preheating, three thermocouples were used to monitor the temperature profile in the regenerative bed with 1/8 inch diameter alumina beads. Figure 19 shows an example of the steady-state temperature cyclic patterns after the initial warm-up at an exhaust gas flow rate of 278 SCFH and an exhaust cycle time of 73s. The oxygen flow rate was 1010 SCFH and the oxygen cycle time was 25s. TC #1 thermocouple, which was the temperature measured at the hot end, swung between 2250 °F and 1650 °F. TC #3, which was the thermocouple installed at the cold end of the regenerator, cycled between 245 °F and 147 °F. Comparing Figure 13 for the nitrogen heating with Figure 19, TC #1 temperature swing in the nitrogen preheating case was smaller and TC #2 and 3 temperature swings in the nitrogen preheating case were larger than those in the oxygen preheating case. The cycle times were the same. The main difference was the exhaust gas flow rate. In the nitrogen preheating case, the exhaust gas flow rate was 359 SCFH which was approximately 30% higher than 278 SCFH used in the oxygen preheating case.

The effects of the cycle time on the temperature profile are shown in Figure 20 as a plot of regenerator temperatures at different cycle times. The hot-end inlet temperatures increased significantly as the oxygen cycle time increased from 10s to 15s cycle time and then flattened

out at 20s and 25s cycle times. The cold-end outlet temperatures did not change much as compared to the cases shown in Figure 13 due to the smaller flow rate of exhaust gas used. The capacity rate ratio of oxygen to exhaust gas was 1.1 in Figure 19 as compared with the capacity rate ratio of nitrogen to exhaust gas 0.7 in Figure 13, which explains the larger temperature swing at the hot end and the smaller temperature swing at the cold end.

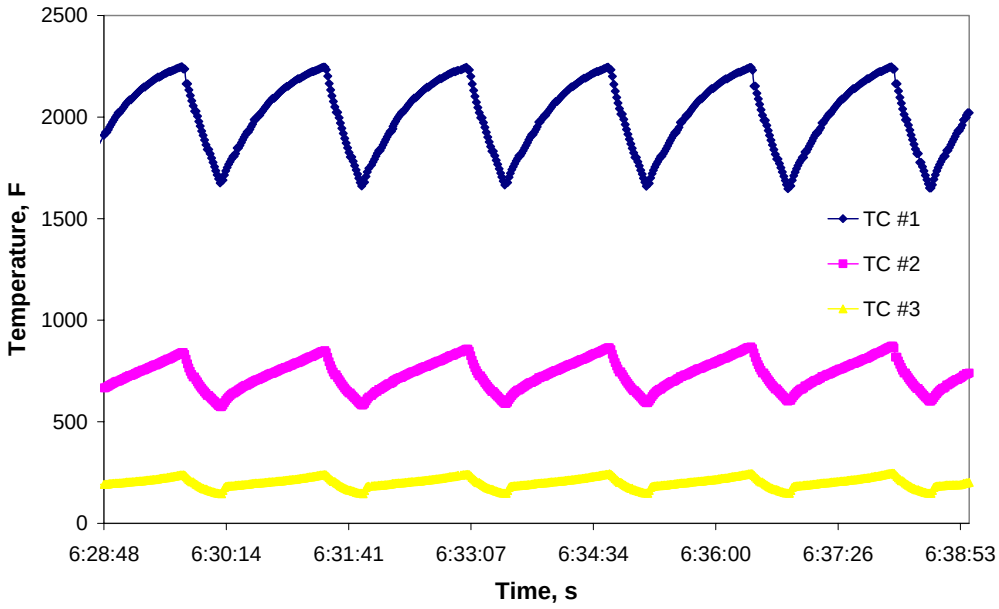

Figure 19. Temperature profile in the regenerator for oxygen preheating

Oxygen preheating tests were designed for both two-bed and four-bed system systems. A regenerative burner system requires at least two regenerative burners to provide continuous firing into the furnace. In a two-bed system when one burner is firing, the other burner is exhausting hot furnace gases to preheat the regenerative bed. Thus the ratio of the exhaust cycle time to the oxygen cycle time is 1, if the reversal/purge times are neglected. The pressure drop through the bed during the exhaust cycle may be relatively large in a two-bed system. In a four-bed system, the hot flue gas can be exhausted through three regenerative beds while only one burner is firing. The exhaust gas flow is divided into three beds and the pressure drop through the bed is reduced significantly. In the present tests with the four-bed system, the ratio of oxygen flow rate to exhaust flow rate was set to approximately 3.6, and the ratio of exhaust cycle time to oxygen cycle time was set to 3. In the two-bed system, the

ratio of oxygen flow rate to exhaust flow rate was set to approximately 1.3, and the ratio of exhaust cycle time to oxygen cycle time was 1. The furnace temperature was maintained at about 2425 °F under all operation conditions except in the case with 630 SCFH of oxygen.

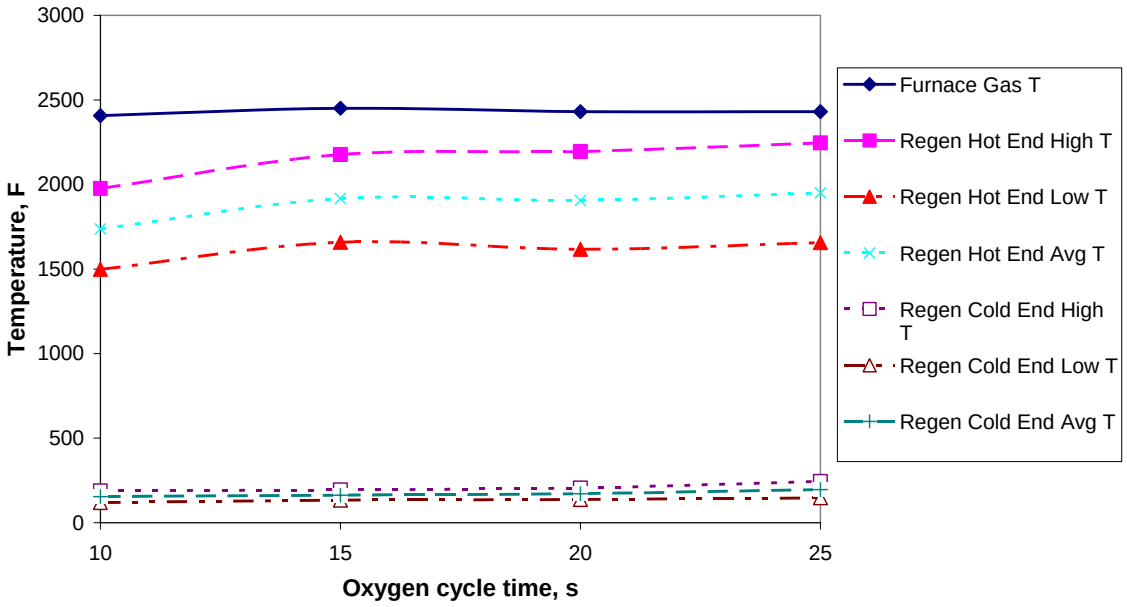

Figure 20. Oxygen cycle time impacts on the regenerator temperature profile

Figure 21 shows the hot-end and cold-end average temperatures for the four-bed system as a function of oxygen cycle time. The hot-end average temperature for the case with an oxygen flow rate of 630 SCFH was lower than the other two flow rates due to the lower furnace temperature. The hot-end average temperature increased from about 1750 °F at oxygen cycle time of 10 s to 1950 °F at 25 s. The cold-end average temperatures increased only slightly from about 170 °F at 10 s to 200 F at 25 s. As discussed previously in the nitrogen preheating tests, the higher preheating temperature at longer cycle time was attributable to an increase in the ratio of the exhaust gas flow volume to the total oxygen flow volume in a cycle.

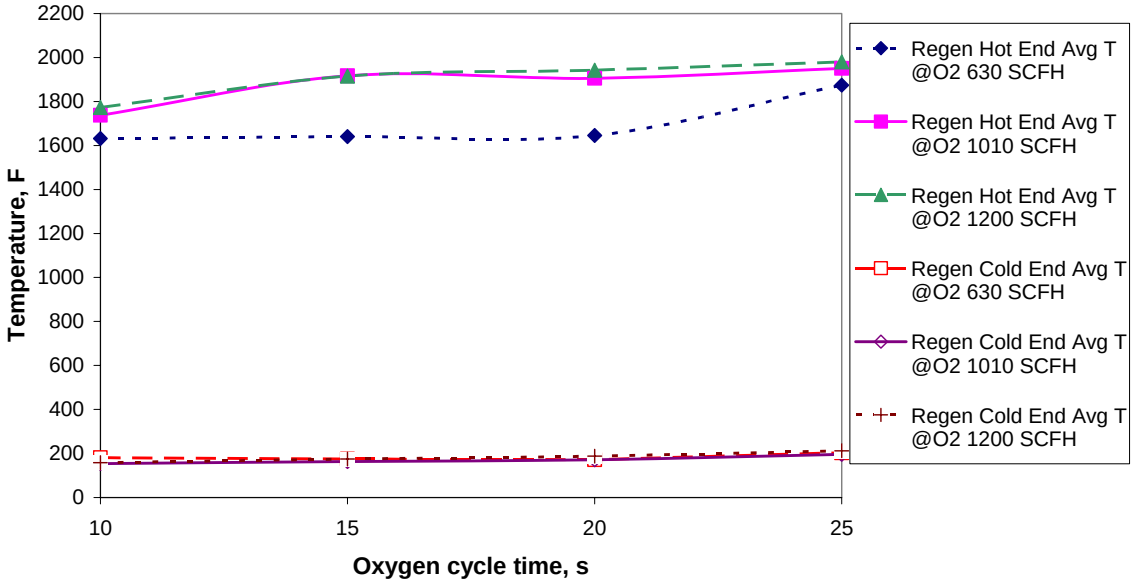

Figure 21. Regenerator temperature profile (ratio of exhaust cycle time and oxygen cycle time=3; ratio of oxygen flow rate and exhaust flow rate=3.6)

Figure 22 presents the hot-end and the cold-end average temperatures for the two-bed system. Both the hot end and the cold end temperatures varied little under the different flow rates in these tests where the ratio of the preheating gas flow rate to the exhaust gas flow rate was kept constant. The hot-end average temperature was significantly lower compared to Figure 21 as the ratio of the exhaust gas flow volume to the total oxygen flow volume in a cycle was lower. The hot-end average temperature increased by about 300 °F from about 1350 °F at oxygen cycle time of 10 s to 1650 °F at 25 s as the ratio of the exhaust gas flow volume to the total oxygen flow volume in a cycle increased more in the two-bed tests.

Figure 23 presents the hot-end average temperatures as a function of the capacity rate ratio of oxygen to flue gas for both two-bed and four-bed simulation tests. For each group of data, the hot-end average temperature decreased significantly as the capacity rate ratio increased.

For an efficient heat recovery, capacity rate ratios close to 1 are desired. If the capacity rate ratio is too low, the flue gas temperature after the regenerators becomes too hot. If the capacity rate ratio is much greater than 1, the oxygen preheat temperature becomes too low

as the amount of the hot flue gas is low. In ideal oxygen-methane combustion, the volume flow rate ratio of exhaust gas and oxygen is 1.5 according to Equation (13) which follows:

$$CH_4 + 2O_2 \rightarrow CO_2 + 2H_2O \quad (13)$$

Since the average molar heat capacities of O_2, CO_2 and H_2O are about 8, 12.05 and 9.4 Btu/lb mol/ F respectively at 2000 ^oF, the capacity rate ratio of oxygen to flue gas is about 0.52, if all of the flue gas from oxy-fuel combustion is exhausted through a regenerator and all of oxygen is preheated in the regenerator. Thus the flue gas temperature after the regenerator becomes too hot. In a practical system only about 50-60% of the flue gas should be introduced to the regenerator to preheat oxygen and the rest of the flue gas should be exhausted separately.

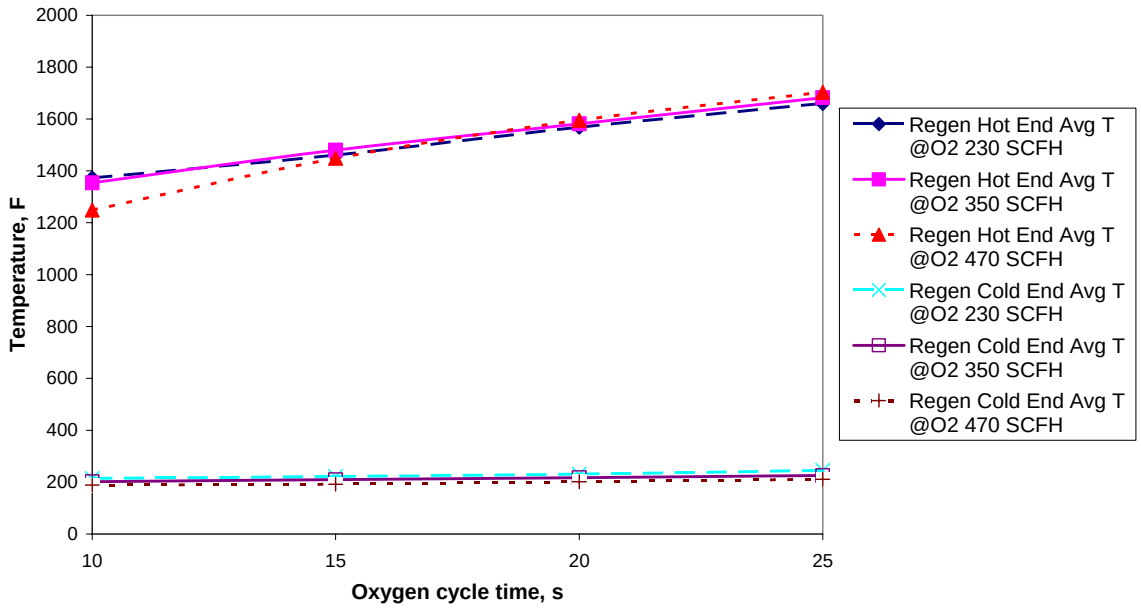

Figure 22. Regenerator temperature profile (ratio of exhaust cycle time and oxygen cycle time=1; ratio of oxygen flow rate and exhaust flow rate=1.3)

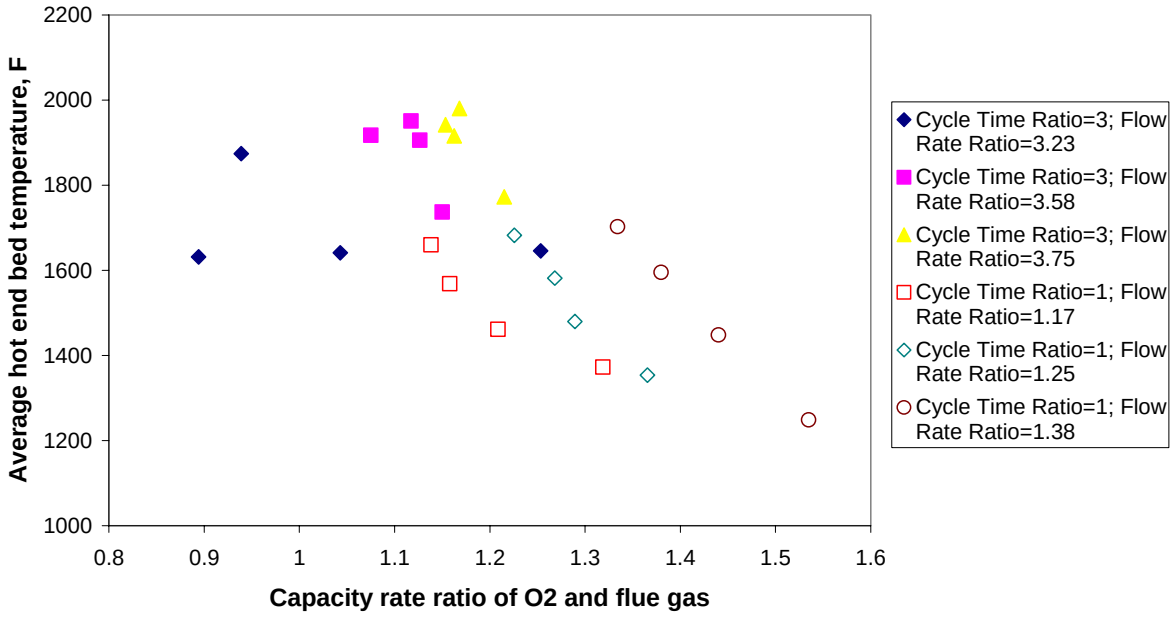

Figure 23. Average hot-end bed temperature at different capacity ratios of O_2 to flue gas

The Λ-Π heat transfer model developed from the N_2 preheating tests can be applied to the O_2 preheating cases by replacing the physical properties of nitrogen with those of oxygen. Figure 24 shows the comparison between the measured values and predicted values of the bed hot end low peak temperature and the cold end high peak temperature when the cycle time ratio was about 1:1, the exhaust gas flow rate was 196 SCFH and the O_2 flow rate was 230 SCFH. The relative error at the hot end was about 3% and at the cold was about 22%. The Λ-Π model offers reasonably good predictions and can be used in the future regenerator design.

Conclusions

Oxygen was preheated up to 2000 °F in the pilot scale regenerator under various flow rates and exhaust gas and oxygen cycle times. The average heat exchange rate increased with the oxygen flow rate and about 15,000 Btu/hr was achieved at the average oxygen flow rate of 300 SCFH at the capacity rate ratio of 1.15. The cycle time did not have a strong impact on the bed temperature profile. The feasibility of oxygen preheating was demonstrated to recover typically 40-60% of the sensible heat available in the flue gas from oxy-fuel combustion. The Λ-Π model offers reasonably good predictions.

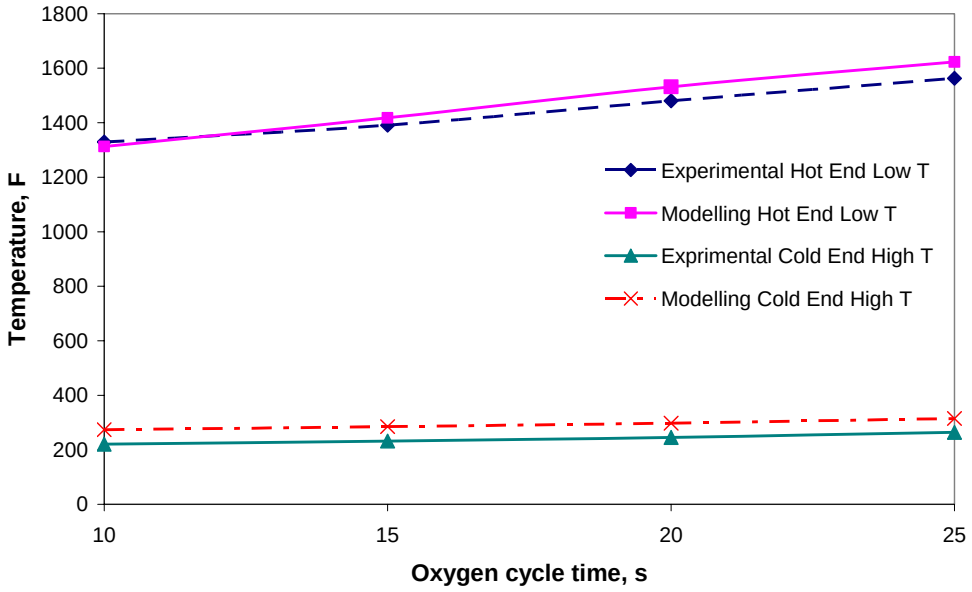

Figure 24. Temperature comparison of experiments and Λ-Π models for O2 preheating

3.3 NATURAL GAS THERMOCHEMICAL REFORMING PILOT TEST

Overview

In oxy-natural gas combustion, physical preheating of natural gas has approximately the same heat recovery capability as oxygen preheating at the same preheat temperature. However, the maximum natural gas preheating temperature is limited to about 350 ^{o}C in practical systems due to cracking of hydrocarbons which results in the fouling of the heat exchanger. One way to avoid the cracking and sooting problems is to mix some of the oxy-fuel combustion flue gas with natural gas and recover more heat through the endothermic CO_2 and steam reforming reactions, as discussed in Chapter 2. The feasibility of the concept has been verified by the bench-top tests under steady-state conditions. The goals of the pilot-scale tests were to evaluate the extent of thermochemical heat recovery in cyclic regenerative systems and to provide the engineering design information for commercial scale up.

Experimental Setup

The design of the regenerative bed for thermochemical heat recovery was the same as that used for the nitrogen or oxygen preheating. The piping arrangement of gases was modified as shown in Figure 25 and Figure 26. Instead of the eductors, a vacuum blower was installed to draw cooled flue gas out of the regenerator in an exhaust cycle and to recycle a portion of the cold flue gas back to the other regenerator as a reforming reactant. The rest of the cold flue gas was exhausted to a stack. As seen in Figure 26 (b), there were only two piping branches connected to each regenerator, i.e., an exhaust gas stream and a reforming gas stream. The nitrogen purge gas was removed. The purge step was conducted by the recycled flue gas through the reforming gas pipe. In a two-bed system, the reforming cycle was designed one second shorter than the exhaust cycle to provide a purge cycle in which natural gas supply was shut off by a solenoid valve and the recycled flue gas continued to flow and purge the regenerator. Following the purge cycle, the regenerator flow was reversed to the exhaust cycle.

To monitor the reforming product compositions, a 1/16-inch stainless steel tubing was installed into the hot end of the regenerator through the rear flange to take product gas samples by a vacuum pump connected to the sample line. The gas sample from the hot end of the regenerator was introduced to a condenser to remove moisture and then to gas analyzers or GC for composition analysis. A solenoid valve was mounted in line to control the sample timing. The valve was opened one second after the start of the regeneration cycle and closed at the end of the regeneration cycle. Therefore, only the reforming product was taken out of the regenerator. The moisture content in the product gas was measured by a dew-point sensor. All solenoid valves used for the exhaust gas, natural gas, reforming reactant and reforming product sample gas lines were controlled by a Modicon control panel.

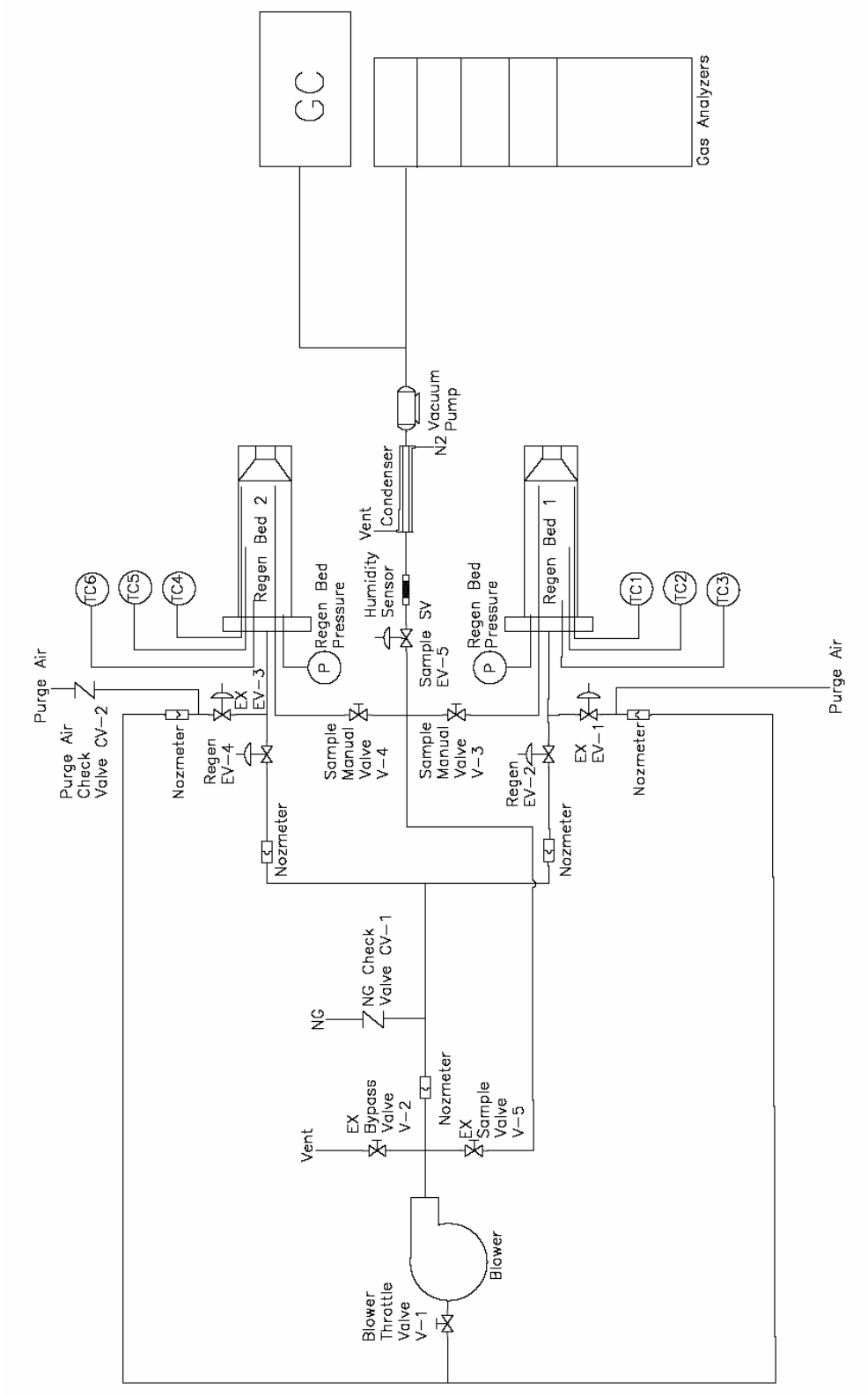

Figure 25. Piping and instrumentation of pilot scale thermochemical regenerators

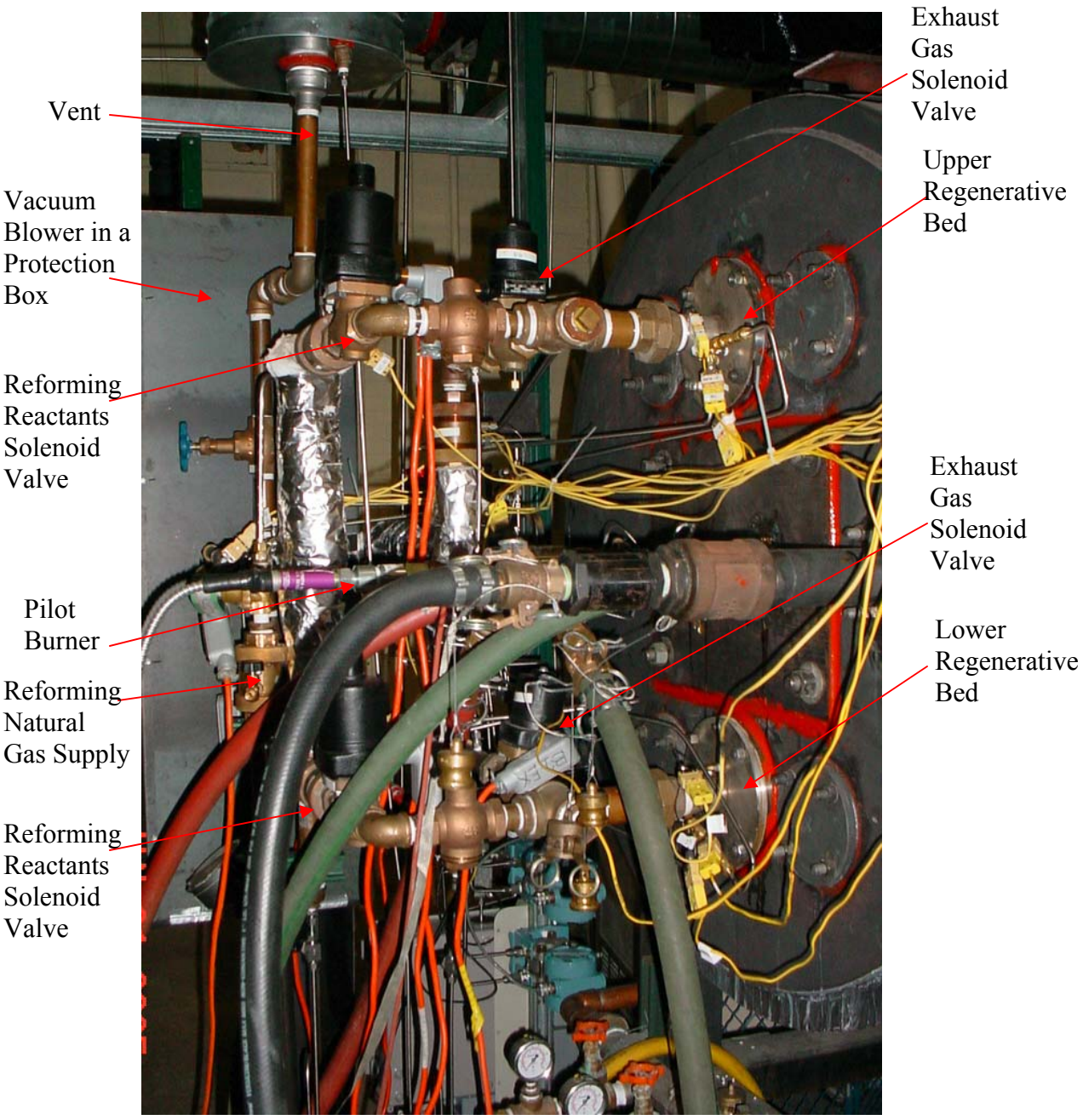
Vent
Vacuum Blower in a Protection Box
Reforming Reactants Solenoid Valve
Pilot Burner
Reforming Natural Gas Supply
Reforming Reactants Solenoid Valve
Exhaust Gas Solenoid Valve
Upper Regenerative Bed
Exhaust Gas Solenoid Valve
Lower Regenerative Bed

(a)

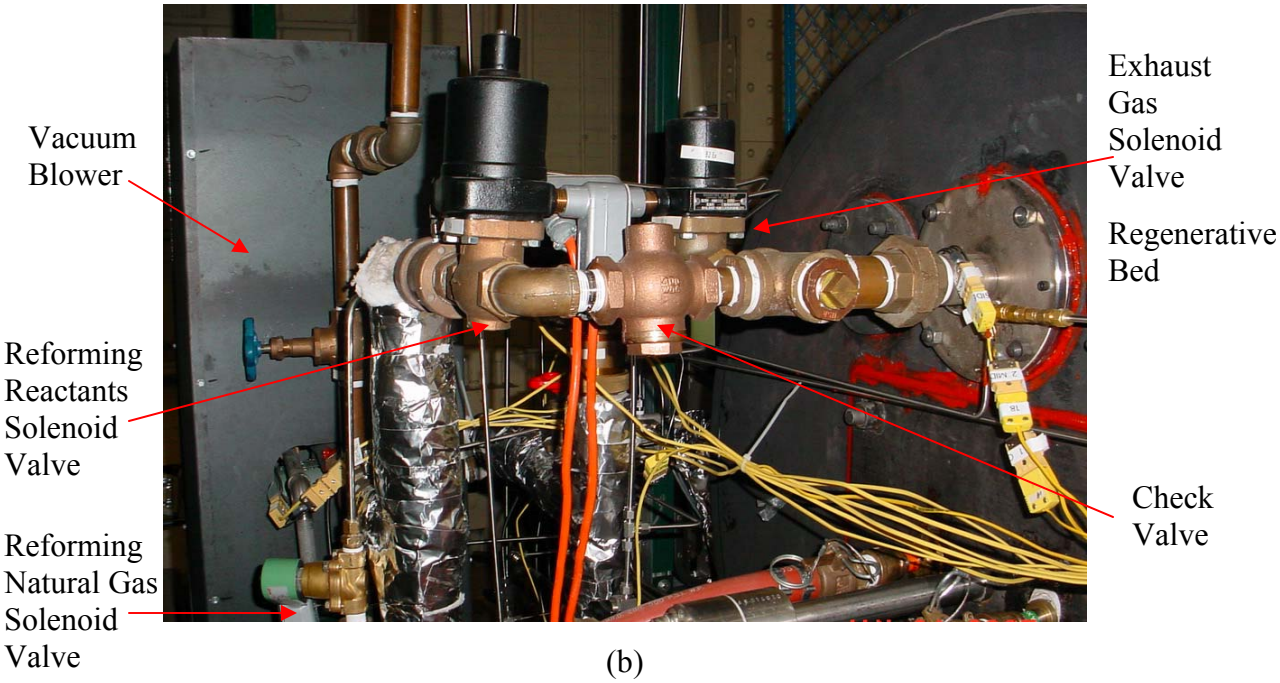

Figure 26. Thermochemical two-bed regenerator system (a) assembly of two-bed system (b) regenerator switching valve system

Design of Experiments and Start up Procedures

The thermochemical regeneration pilot test was designed for a two-bed system.

Five different cycles were tested:

(1) 5s exhaust / 4s regeneration / 1s purge,

(2) 10s exhaust / 9s regeneration / 1s purge,

(3) 15s purge / 14s regeneration / 1s purge,

(4) 20s exhaust / 19s regeneration / 1s purge, and

(5) 25s exhaust / 24s regeneration / 1s purge.

The flow rates of total exhaust gas and natural gas had two levels. At the low flow rate level, the total exhaust gas was approximately 410 SCFH and the natural gas was 84 SCFH. At the high flow rate level, the total exhaust gas was approximately 690 SCFH and the natural gas flow rate was 199 SCFH. At each flow rate level, three different mixing ratios of the recycled flue gas and natural gas (1:1, 0.5:1 and 1.5:1) were tested.

In order to optimize the regenerator performance, six different arrangements of bed materials were tested: (1) 1/8 inch diameter alumina beads, (2) combination of alumina beads and 304 stainless steel beads, (3) cordierite honeycomb, (4) combination of cordierite honeycomb and 304 stainless steel beads, (5) silicon carbide (SiC) foam, and (6) combination of silicon carbide foam and 304 stainless steel beads. Bed materials were packed into the same cylindrical regenerators with 3 1/2-inch in diameter and 5 5/8-inch in length. The physical properties of the bed materials and the bed properties are summarized in Tables 1 and 2, respectively. For the composite beds, the high temperature half of the regenerator was packed with ceramic materials and the low-temperature half was packed with metallic materials. The heat capacity of the stainless steel bed is higher than those of ceramic materials and the overall bed heat capacities increased for composite beds.

To start the reforming experiment, the furnace was preheated to above 2400 °F by the oxy-natural gas pilot burner. The oxygen flow rate of the pilot burner was increased to provide a sufficient amount of oxygen to completely combustion of the additional fuel to be injected into the regenerator. Then the flue gas recycle fan and the regenerator control system were turned on. The natural gas stream for reforming was introduced into the recycled flue gas and injected into the heated regenerator for cyclic operation.

Table 1. Thermal properties of regenerator heat storage materials

	Al_2O_3	SS304	Cordierite	SiC
Thermal conductivity (W/m-K)	6.3	16.2	2.5	77
Density (Kg/m^3)	3960	8000	2300	3100
Heat capacity (J/Kg-°C)	850	500	900	670

Table 2. Regenerator bed properties

Bed material	Bed volume (m^3)	Bulk density (Kg/m^3)	Heat capacity of bed (J/°C)	Specific surface area (m^{-1})
Al_2O_3	8.86E-4	1595	1202	707
Al2O3 + Stainless Steel	4.43E-4 4.43E-4	1595 4614	601 1023	707 707
Cordierite honeycomb	8.86E-4	553	441	1614
Cordierite honeycomb + Stainless Steel	4.43E-4 4.42E-3	553 4614	221 1023	1614 707
Silicon Carbide	8.86E-4	412	245	1046
Silicon Carbide + Stainless Steel	4.43E-4 4.43E-4	412 4614	123 1023	1046 707

Results and Discussions

Figure 27 shows the steady-state cyclic temperature profiles with the alumina beads at the operation conditions of 24s reforming cycle time, total exhaust flow rate of 397 SCFH, recycled exhaust gas flow rate of 104 SCFH, and natural gas flow rate of 84 SCFH. Similar temperature profiles were observed in other thermochemical regeneration conditions. Compared with Figures 13 and 19 for nitrogen and oxygen preheating cases, thermochemical regeneration exhibited a few distinct features. The hot-end temperature TC #1 fluctuated over 500 °F between 1960°F to 1460 °F, and at the end of the regeneration cycle, TC #1 temperature was slightly lower than TC #2, the temperature measured in the middle of the regenerator. The dramatic temperature change in the high-temperature section was clearly caused by the endothermic natural gas reforming reactions. TC #2 was almost flat at 1500 °F and TC #3, the temperature at the cold end of the regenerator, cycled between 820 °F and 680 °F.

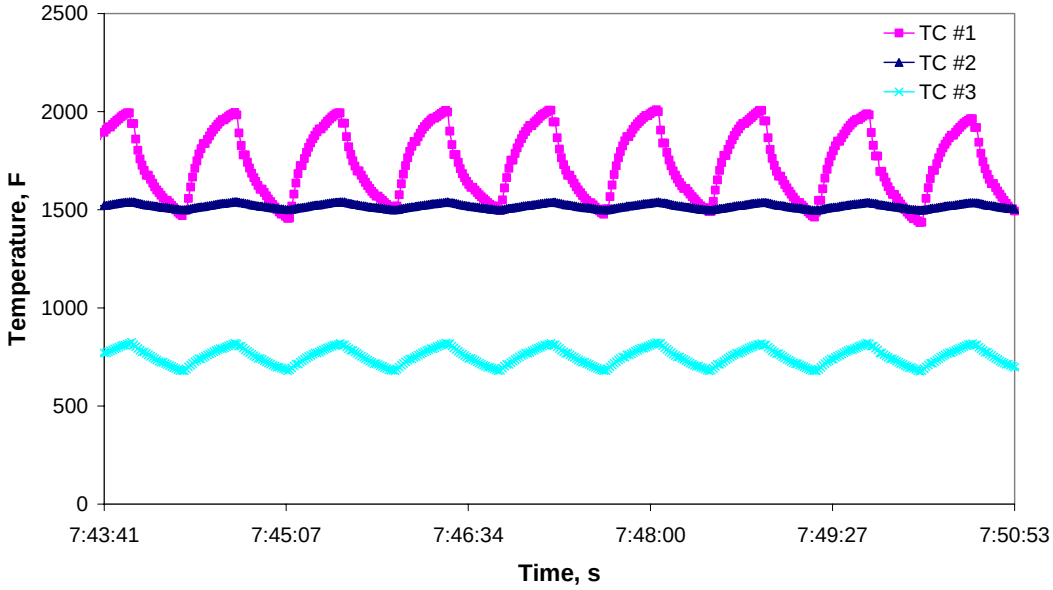

Figure 27. Temperature profile in thermochemical regenerator

The average TC #3 temperature was much higher than those of nitrogen and oxygen preheating tests for two reasons. The flow rate ratios of cold fluid to hot fluid were much lower and the inlet temperature of the cold fluid was higher due to recycling of warm flue gas. Typical temperature of recycled flue gas was about 200-220 °F and the reforming reactant temperature was about 165 °F in the experiment. Overall, the average regenerator temperature was higher which helped to promote the reforming reactions. The temperature in the exhaust pipe was 310 °F due to both the heat losses from the pipings downstream of the regenerators and the additional regenerative heat exchange taking place through the piping components. Although the sharp temperature drop of the flue gas after the regenerator kept the temperature of the exhaust pipe within the acceptable operation, the temperature range for this small-scale test and the temperature at the cold end of the regenerator, (which cycled between 820 °F and 680 °F), is considered too high for full-scale commercial regenerative systems.

Figure 28 is the regenerator temperature profiles under different cycle times. The operation conditions were: total exhaust gas flow rate 400 SCFH, recycled exhaust gas flow rate 55 SCFH, natural gas flow rate 84 SCFH, furnace gas temperature 2370 °F, and reforming

reactant temperature 146 °F. The hot end high temperature increased and the hot-end low temperature decreased with the rising cycle time as the temperature fluctuation expanded with the cycle time. The cold-end low temperatures were relatively constant and the cold end high temperature increased as the cycle time increased.

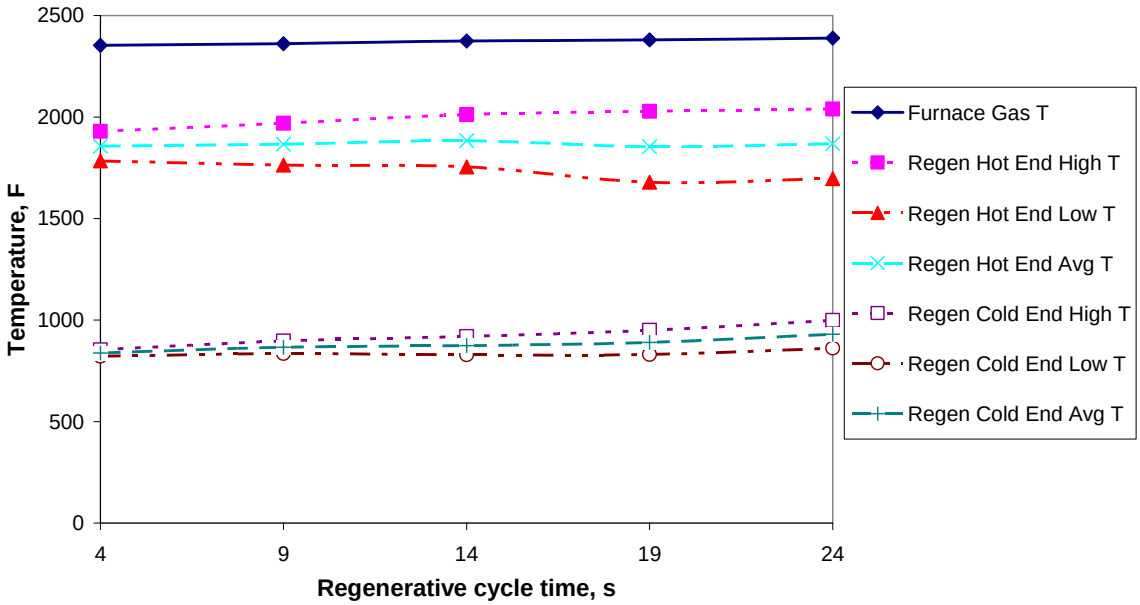

Figure 28. Cycle time impacts on thermochemical regenerator temperature profile

Figure 29 illustrates the reforming product compositions (wet basis) under the same operation conditions as Figure 28. As the regeneration cycle time increased, CH_4 and CO_2 concentrations declined, H_2 and CO concentrations increased, and the overall CH_4 conversion increased. The higher conversion rates observed at longer cycle times were due to higher average bed temperatures. As previously discussed in nitrogen preheating tests, the flow rate ratio of the reforming mixture and the exhaust gas increased slightly with the cycle time. When the regeneration cycle time was 24s, the product gas compositions were: CH_4 36%, H_2 18%, CO 13%, CO_2 10%, and H_2O 18%.

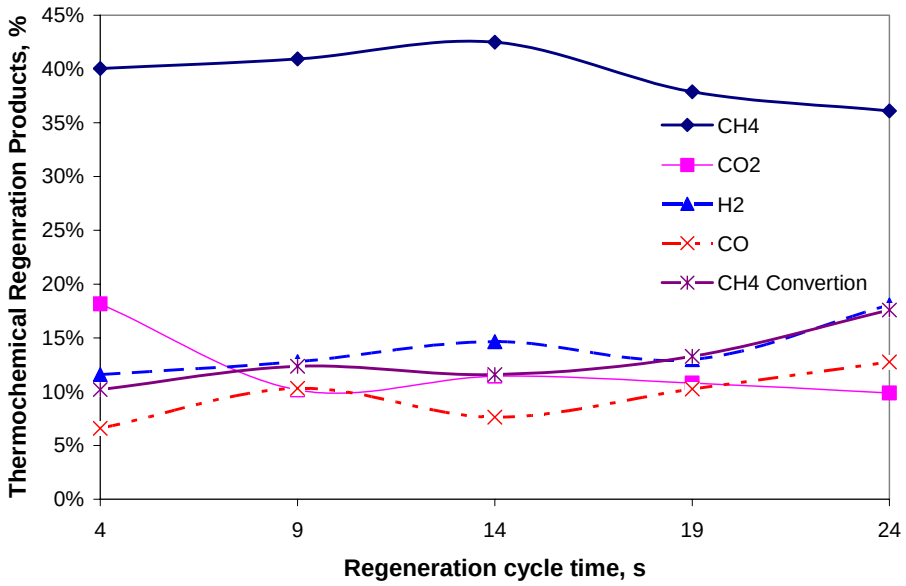

Figure 29. Alumina bead thermochemical regenerator products under different cycle times

Figure 30 shows the measured temperature profiles at three different mixing ratios of 0.65, 1.24 and 1.56. In all three cases, natural gas flow rate and the total exhaust gas flow rate were 84 SCFH and 410 SCFH respectively, and the regeneration cycle time was 24s. The reforming reactant inlet temperature increased with the mixing ratio because more recycled flue gas with higher sensible heat was blended with the same amount of natural gas. The regenerator temperature dropped with the increasing mixing ratio, as the ratio of the reforming reactant flow rate to the exhaust gas flow rate decreased at a higher mixing ratio.

Figure 31 shows a comparison of the gross heat exchange rate and the net heat exchange rate for three different flue gas mixing ratios. The gross heat exchange rate is defined as "the average heat exchanged in a single regenerator per hour". When flue gas is recycled through a regenerator, a portion of the heat exchange capacity of the regenerator is used to re-heat the cooled flue gas back to the furnace flue gas exhaust temperature. The net heat exchange rate was calculated by subtracting the heat consumed to re-heat the recycled flue gas from the gross heat exchange rate. As more flue gas was recycled through the regenerators and the mixing ratio of flue gas to natural gas was increased from 0.5 to 1.6, the gross heat exchange rate increased from about 17,000 Btu/hr to over 19,000 Btu/hr. The net heat exchange rate,

however, decreased with increasing flue gas recycle. Thus it is desirable to minimize the amount of flue gas recycle required.

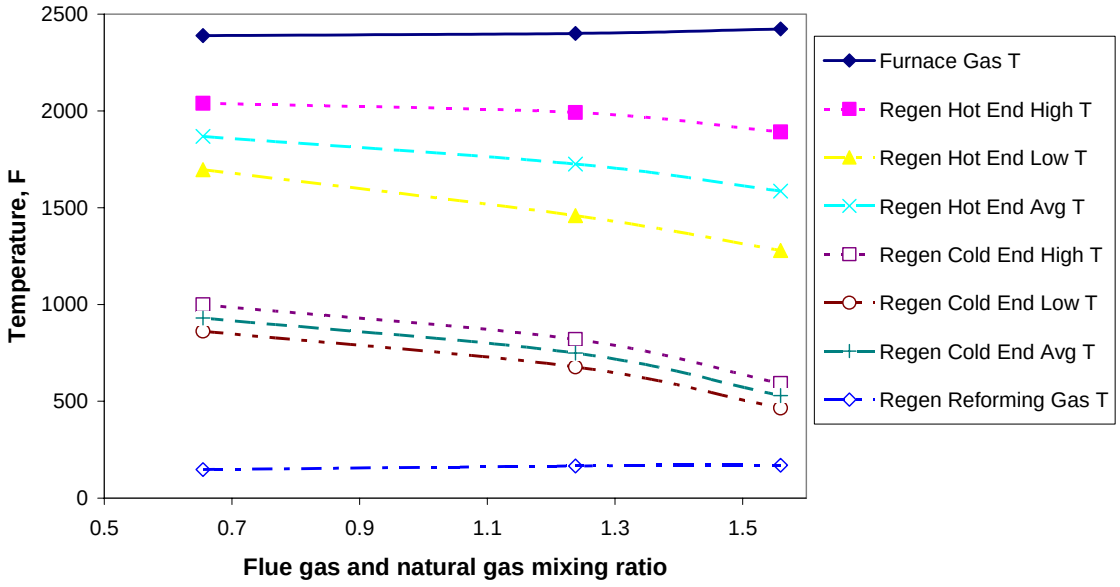

Figure 30. Alumina bead thermochemical regenerator temperatures under different flue gas and natural gas mixing ratios

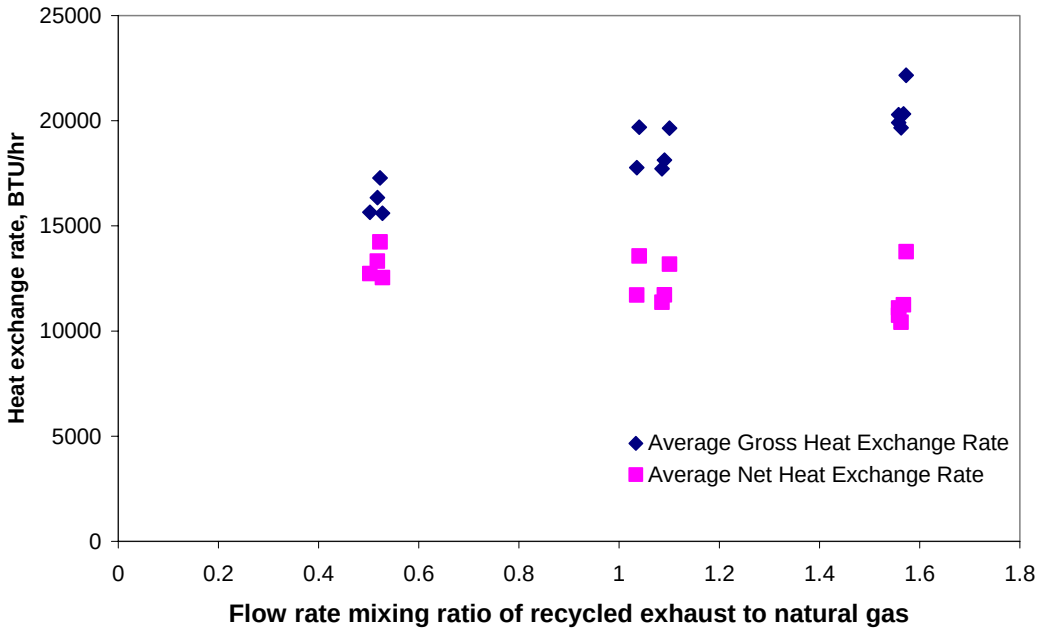

Figure 31. Heat exchange rate vs. mixing ratio for high natural gas flow rate tests

Figure 32 shows the gross heat exchange rate and the net heat exchange rate from all the test runs as a function of the flow rate ratio of the actual exhaust gas flow rate minus the recycle flue gas to the theoretically available exhaust gas flow rate from the stoichiometric combustion of natural gas and oxygen used for the regen burner. The flow rate ratio of 1 corresponds to the case that all of the flue gas from the regenerative burner is exhausted through the regenerative burner. One of the unique features of the thermochemical regenerator is to be able to recover extra waste heat from other burners in the same furnace. For example, flow rate ratio of 1.5 corresponds to the case that 50% more flue gas than its own flue gas is introduced to the regenerator. The heat exchange rate generally increased with the flow rate ratio under the same natural gas flow rate. Heat exchange rates were much higher under high natural gas flow rates and gross heat exchange rates over 20,000 Btu/hr were achieved in some cases. However, the net heat exchange rate was below 15,000 Btu/hr for all cases.

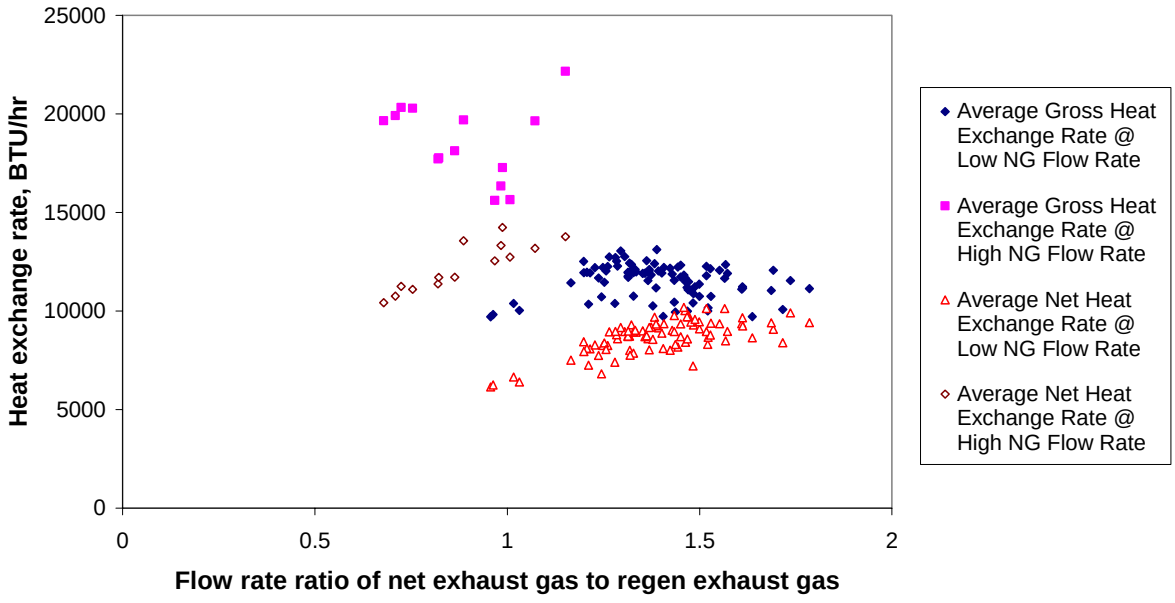

Figure 32. Heat exchange rates for thermochemical regeneration tests - all test runs

Figure 33 shows the product compositions on a wet basis under the above mixing ratios. As the mixing ratio increased, methane concentration dropped slightly, CO_2 increased dramatically, and H_2 and CO decreased substantially. These changes were caused both by the dilution effect by mixing greater amounts of flue gas, which consists of mostly CO_2 and H_2O, and also by reduced reforming reactions at higher mixing ratios. Since the mixing ratio in the experiment was controlled by varying the recycled flue gas flow rate, both the gas residence time and the average bed temperature decreased at higher mixing ratios which reduced methane conversion. At the mixing ratios of 0.65, 1.24 and 1.56, methane conversion rates were 18%, 12% and 8% respectively.

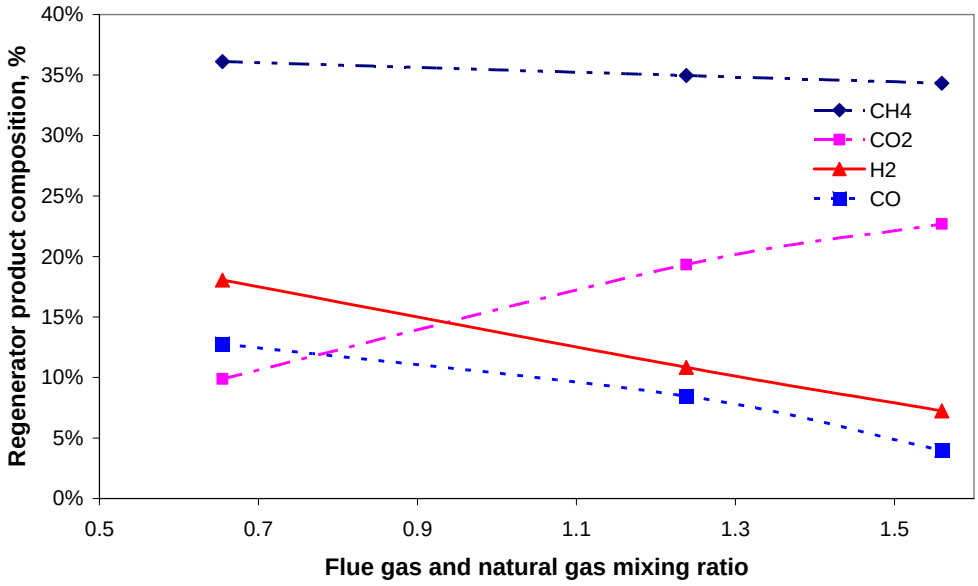

Figure 33. Alumina bead thermochemical regenerator product compositions under different flue gas and natural gas mixing ratios

The total heat recovery capability of the reforming reactants consists of chemical heat absorption from the reforming reactions and physical heat absorption from the sensible heat increase of the reforming gases.

Figure 34 presents the net heat exchange rate and the split between the thermal and chemical heat recovery components. The “cold side” exchange rates were calculated based on the flow

rates of natural gas and recycled flue gas and the measured gas composition at the hot end of the bed at the TC #3 location for relative comparison. Thus these heat exchange rates are substantially less than the "hot side" values calculated as the heat released from the exhaust gases. The net heat exchange rate was slightly greater at the mixing ratio of 1.24, but approximately the same for all three mixing ratios. However, the split between the thermal and chemical heat recovery components varied dramatically. At the low mixing ratio, the fraction of chemical heat recovery component was 50% of the total. While at the high mixing ratio, the fraction of chemical heat recovery component decreased to about 25%. Although the volume of the reforming gas was much lower under the low mixing ratio, the total amount of heat exchanged was similar due to increased endothermic chemical reactions. This self-adjusting feature of the thermochemical regeneration is a unique characteristic as compared to the conventional regenerative heat recovery systems.

Table 3 lists typical data on regenerator performance under two different flow rates at a reforming cycle time of 14s and the mixing ratio of the recycled exhaust gas to natural gas of approximately 1.

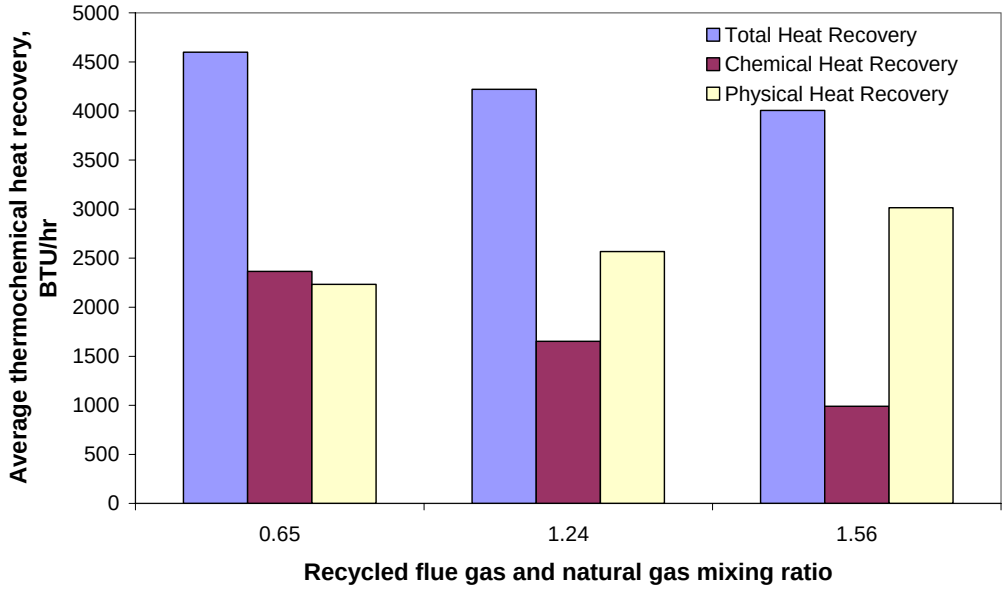

Figure 34. Alumina bead thermochemical regenerator heat recovery under different flue gas and natural gas mixing ratios

Table 3. Thermochemical regeneration at different flow rates

	Low flow rate	High flow rate
Total exhaust flow rate (SCFH)	401	673
Recycled exhaust flow rate (SCFH)	100	216
Natural gas flow rate (SCFH)	84	199
Exhaust cycle time (s)	15	15
Regeneration cycle time (s)	14	14
Furnace gas temperature (F)	2395	2400
Regen hot end high peak temperature (F)	1917	2115
Regen hot end low peak temperature (F)	1520	1264
Regen hot end temperature swing (F)	397	851
Regen cold end high peak temperature (F)	806	748
Regen cold end low peak temperature (F)	717	606
Regen cold end temperature swing (F)	89	142
CH_4% in reforming product (wet)	36%	44%
H_2% in reforming product (wet)	11%	3%
CO% in reforming product (wet)	8%	4%
CH_4 conversion	12%	4%
Reforming reactants residence time (ms)	56	26
Average Gross Heat Exchange Rate (BTU/hr)	10384	17718
Average Net Heat Exchange Rate (BTU/hr)	7399	11368
Flow rate ratio of actual net exhaust to exhaust from oxy-fuel regen	1.28	0.82
Heat transfer ratio of actual net exhaust heat recovery to exhaust heat from oxy-fuel regen	0.99	0.64

In Figure 35, the methane conversion results of the pilot-scale experiments are compared with the predictions based on the bench-top experiments, using the empirical reaction kinetics developed from the bench-top tests, i.e., Equation (4). The hot-end average temperature was used for the reaction temperature. In the pilot-scale experiments, the heat storage media was 1/8-inch diameter alumina bead, the reforming natural gas flow rate was 84 SCFH and the mixing ratio of exhaust gas to natural gas was about 1:1. The residence time in the regenerator was about 50 ms. At the reforming cycle times of 5s and 10s, the discrepancies between the pilot-test results and empirical predictions were relatively large. At the cycle times of 15s, 20s and 25s, the agreements were much better.

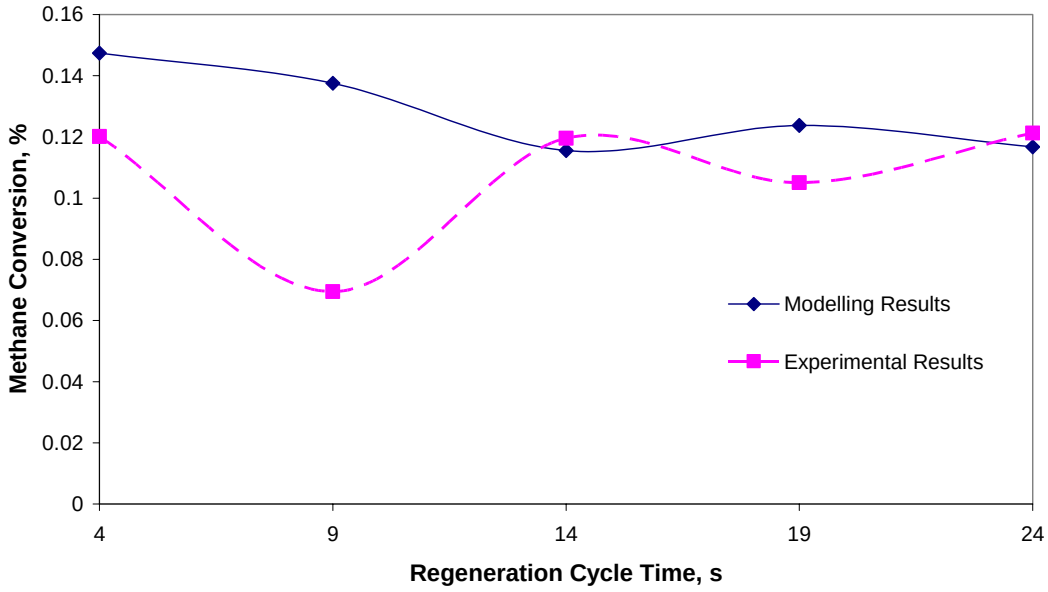

Figure 35. Methane conversion comparison between modeling and experiments

The poor predictions at the regeneration cycle time (5s and 10s) resulted from the reaction temperature, as the reforming reactions are highly temperature sensitive. The average hot-end temperature of the regenerator was below the applicable range of Equation (4), i.e., lower than 1800 ºF. The empirical equation also showed poor fits for other out-of-the-range operational conditions, such as the mixing ratio of 0.5:1 and 1.5:1, and honeycomb heat storage media. Thus,Equation (4) could be used as a predictive tool only within the specified range of correlation.

In order to correlate the pilot-scale data for a wider operation range Equation (14) was derived using the same empirical formulation.

$$X_{CH_4} = \exp(1193.50 + \frac{1566.16}{T}) f_{CH_4,0}^{27.77} f_{CO_2,0}^{1588.52} f_{H_2O,0}^{-1488.40} S_v \tau \quad (14)$$

R-squared value for the curve fitting is 0.8. The error is larger than the bench-top model since the same number of curve fitting variables was applied and a wider variable range was covered. The above equation is suitable for temperatures between 1300 ºF to 2000 °F, residence times between 23 ms to 230 ms, and reforming reactant mixing ratios of flue gas to natural gas between 0.5:1 to 1.5:1.

Figure 36 compares the heat recovery efficiencies of different bed materials and configurations. The Y-axis is the ratio of the net heat exchange rate to the waste heat available from the combustion products of the natural gas (with oxygen) injected from the regenerator. The X-axis is the flow rate ratio of the actual net exhaust gas flow rate to the theoretically available exhaust gas-flow rate from the stoichiometric combustion of natural gas and oxygen used for the regenerator. The 45-degree line represents the perfect heat recovery where 100% of the sensible heat in the net exhaust gas (i.e., actual minus the recycled flue gas) through the regenerator is recovered and the exhaust gas cools down to the ambient temperature. The data points closer to the 45-degree line indicate better heat recovery efficiencies. Data from six different bed materials and configurations are shown in the figure.

The composite bed of cordierite honeycomb and 304 stainless steel beads showed best results followed by the composite bed of silicon carbide foam and 304 stainless steel beads. The bed of alumina beads was shown to be least efficient. Since both cordierite honeycomb and silicon carbide foam have much higher specific surface areas, the heat transfer efficiencies were higher than those for alumina beads. The composite beds achieved better results as the overall heat capacity of the bed increased due to the higher heat capacity and conductivity of stainless steel beads.

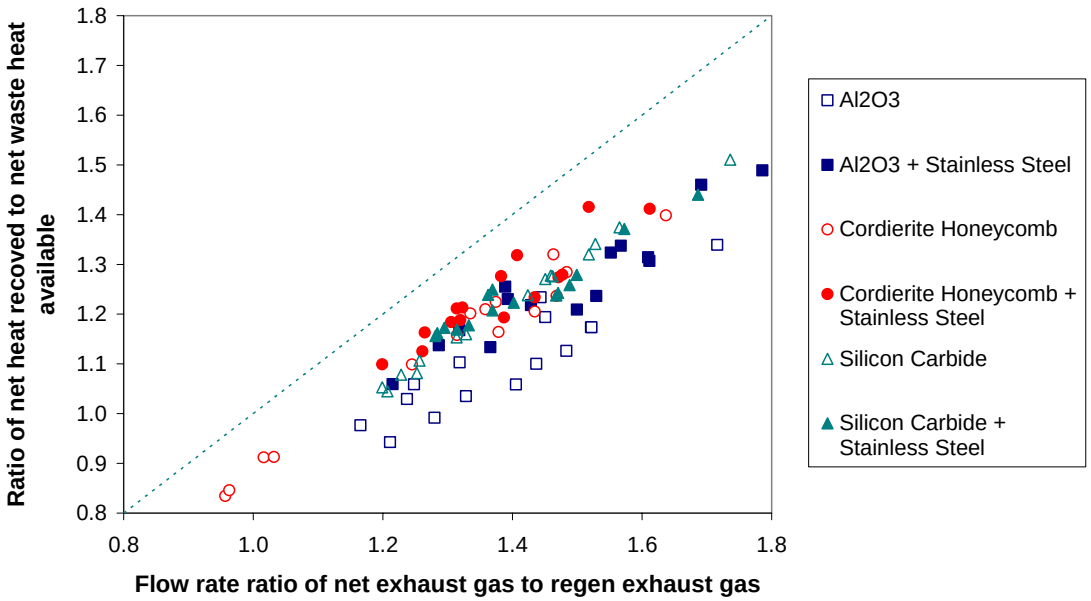

Figure 36. Performance of different thermochemical regenerators

Table 4 shows a detailed comparison of the performance of an alumina bed and a composite bed. The composite bed had the same refractory shell as the alumina bed. Inside, the bed was packed half with 1/8 inch diameter alumina beads and half with 1/8 inch SS304 beads. When furnace gas temperature was similar, both the hot-end average temperature and the cold-end average temperature were approximately 150 °F lower in the composite bed than in the alumina bed. Since stainless steel has a much higher thermal conductivity than alumina, the heat transfer resistance between gas and bed was reduced. Since the regenerator average temperature was lower in the composite bed, the reforming reaction was suppressed a little and natural gas conversion was 4% lower.

Table 4. Comparison of ceramic and ceramic-metallic regenerator materials

	Alumina bed	Composite bed
Heat storage media material	1/8" Al_2O_3 beads	Half is 1/8" Al_2O_3 beads; Half is 1/8" Stainless Steel beads
Total exhaust flow rate (SCFH)	400	416
Recycled exhaust flow rate (SCFH)	56	57
Natural gas flow rate (SCFH)	84	84
Exhaust cycle time (s)	20	20
Regeneration cycle time (s)	19	19
Furnace gas temperature (F)	2380	2375
Regen hot end high peak temperature (F)	2028	1723
Regen hot end low peak temperature (F)	1679	1692
Regen hot end average temperature (F)	1854	1708
Regen cold end high peak temperature (F)	950	743
Regen cold end low peak temperature (F)	830	736
Regen cold end average temperature (F)	890	739
Regen exhaust pipe temperature (F)	313	253
CH_4% in reforming product (wet)	38%	49%
H_2% in reforming product (wet)	13%	9%
CO% in reforming product (wet)	10%	10%
CH_4 conversion	13%	9%
Average Gross Heat Exchange Rate (BTU/hr)	9938	10747
Average Net Heat Exchange Rate (BTU/hr)	8293	9094
Flow rate ratio of actual net exhaust to exhaust from oxy-fuel regen	1.44	1.50
Heat transfer ratio of actual net exhaust heat recovery to exhaust heat from oxy-fuel regen	1.10	1.21

Figure 37 compares the relative amounts of heat recovered and the heat recovery efficiencies of oxygen preheating and natural gas reforming. In oxygen preheating, the maximum ratio of heat recovered to the waste heat available in the combustion products of the regen burner was limited about 0.65. In natural gas reforming, the maximum recovery ratio was over 1.5. The heat recovery efficiencies were generally much better with oxygen preheating, i.e., the data points were closer to the 45-degree line, as the flue gas exhaust temperature after the regenerator was kept low by limiting the intake of the exhaust gas flow rate relative to the oxygen flow rate.

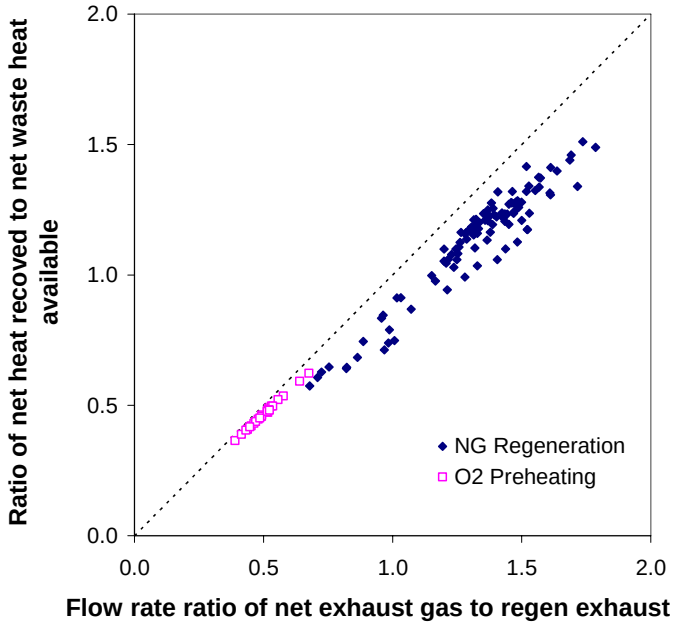

Figure 37. Comparison of O2 preheating and natural gas thermochemical regeneration heat recovery performances

In the thermochemical regenerator tests, some soot was found in the exhaust gas pipe. It is believed that soot was generated by cracking of natural gas during the regeneration cycle inside the regenerator. As the gas flow was reversed in the exhaust cycle, some of the soot was carried over into the exhaust pipe and deposited there. The problem has to be solved for the design of the commercial regenerative systems. A soot cleaning step using purge gas containing oxygen to burn off soot was previously suggested in Reference 9, but was not tested due to the limited scope of this project.

Summary

The feasibility of the thermochemical heat recovery concept was demonstrated by reforming natural gas and recycled flue gas in the pilot-scale regenerators. Gross heat exchange rates over 20,000 Btu/hr were achieved in some cases, but the net heat exchange rate was below 15,000 Btu/hr for the test conditions due the extra heat required to re-heat the recycled flue gas. The flue gas temperature after the regenerator was generally higher for these tests and further improvements may be possible for commercial systems. A unique feature of the thermochemical regenerator is to recover extra waste heat from other burners. The tests demonstrated that the heat recovery capability was over 150% of the waste heat available from its own flue gas. Of the six different bed materials and configurations tested, the composite bed of cordierite honeycomb and 304 stainless steel beads showed the best results. Some soot was found in the exhaust gas pipe and the problem has to be solved for the design of future commercial regenerative systems.

REFERENCES

[1] Kobayashi, H., "Segregated Zoning Combustion", U.S. 5076779, December 31, 1991.

[2] Ryan, H.M., Francis, A.W., Riley, M.F., and Kobayashi, H., "Dilute Oxygen Combustion" Phase I Report for U.S. Dept. of Energy (DOE/ID/13331-T1, October, 1997

[3] M.F. Riley, H.M. Ryan, and H. Kobayashi "Applications of Dilute Oxygen Combustion (DOC) Technology for Steel Reheating Furnaces", American Flame Research Committee (AFRC) International Symposium, Newport Beach, CA, USA, September 2000

[4] Ryan III, H.M., Francis Jr., A.W., Riley, M.F., and Kobayashi, H., "Low NOx Combustion Process", U.S. 6007326, December 28, 1999.

[5] Ryan, H.M., Francis, A.W., Riley, M.F., and Kobayashi, H., "Dilute Oxygen Combustion" Phase I Report for U.S. Dept. of Energy (DOE contract number DE-FC07-95ID13331), October, 1997

[6] Riley, M.F., "Dilute Oxygen Combustion" Phase III Report for U.S. Dept. of Energy (DOE contract number DE-FC07-95ID13331), May, 2000

[7] Riley, M.F., "Dilute Oxygen Combustion – Optimized Reheat Furnace Design" Phase IV Report for U.S. Dept. of Energy (DOE contract number DE-FC07-95ID1333), April, 2003

[8] Schmidt, F.W., and Willmott, A.J., "Thermal Energy Storage and Regeneration", Hemisphere Publishing Corporation, New York, 1981.

[9] H. Kobayashi, "Thermochemical Regenerative Heat Recovery Process", U.S. Patent 6,113,874, September 5, 2000.

[10] Xu, J., and Froment, G.F., "Methane Steam Reforming, Methanation and Water-Gas Shift: I. Intrinsic Kinetics", AICHE Journal, Vol. 35, No. 1, pp. 88-103, 1989.

[11] Snoeck, J.W., and Froment, G.F., "Steam/CO_2 Reforming of Methane. Carbon Filament Formation by the Boudouard Reaction and Gasification by CO_2, by H_2, and by Steam: Kinetic Study", Ind. Eng. Chem. Res., Vol. 41, pp. 4252-4265, 2002.

[12]Choudhary, V.R., and Rajput, A.M., "Simultaneous Carbon Dioxide and Steam Reforming of Methane to Syngas over NiO-CaO Catalyst", Ind. Eng. Chem. Res., Vol. 35, pp. 3934-3939. 1996.

[13] Snoeck, J.W., and Froment, G.F., "Steam/CO_2 Reforming of Methane. Carbon Formation and Gasification on Catalysts with Various Potassium Contents", Ind. Eng. Chem. Res., Vol. 41, pp. 3548-3556, 2002.

[14] Verykios, X. E., "Catalytic Dry Reforming of Natural Gas for the Production of Chemicals and Hydrogen", Industrial Journal of Hydrogen Energy, Vol. 28, pp. 1045-1063, 2003.

[15] Wang, S., and Lu, G.Q., "Carbon Dioxide Reforming of Methane to Produce Synthesis Gas over Metal-Supported Catalysts: State of the Art", Energy & Fuel, Vol. 10, pp. 896-904, 1996.

[16] Verkhivker, G., and Kravchenko, V., "The Use of Chemical Recuperation of Heat in a Power Plant", Energy, Vol. 29, pp. 379-388, 2004.

[17] Paisley, M.A., "Method for Hot Gas Conditioning", U.S. 5494653, February 27, 1996.